Title

Design, Manufacture, and Analysis of a GOx/Nylon 6 Hybrid Rocket Propulsion System with a Hydrogen Co-firing Configuration

Author

Cameron, Austin Beau

Publication Date

2022

Peer reviewed|Thesis/dissertation

Design, Manufacture, and Analysis of a GOx/Nylon 6 Hybrid Rocket Propulsion System with a Hydrogen Co-firing Configuration

By

AUSTIN CAMERON
THESIS

Submitted in partial satisfaction of the requirements for the degree of

MASTER OF SCIENCE

in

Mechanical and Aerospace Engineering

in the

OFFICE OF GRADUATE STUDIES

of the

UNIVERSITY OF CALIFORNIA

DAVIS

Approved:

Paul Erickson, Chair

Valeria La Saponara

Ben Shaw

Committee in Charge

2022

CONTENTS

List of Figures

List of Equations

Abstract

Design, Manufacture, and Analysis of a GOx/Nylon 6 Hybrid Rocket Propulsion System with a Hydrogen Co-firing Configuration

As hybrid rocket propulsion systems continue to be utilized as launch solutions within the small satellite industry, their inherit poor fuel regression rates and low combustion efficiencies possess a notable threat to mission performance. This body of work investigates the practicality of hydrogen co-firing as a novel technique to combat these deficiencies. A hybrid rocket propulsion system of gaseous oxygen (GOx) and nylon 6 thermoplastic fuel grain with a gaseous hydrogen (GH_2) co-firing configuration was designed and manufactured for preliminary analysis in understanding the internal ballistic effects of hydrogen addition. In order to appropriately characterize the overall combustion event, comprised of both the GOx/nylon 6 and GOx/GH_2 burn, NASA CEA (Chemical Equilibrium with Applications) software was utilized. The baseline burning of GOx and nylon 6 yielded a simulated combustion efficiency of 85.67% and an overall system efficiency of 85.95%. The simulated GOx and GH_2 burn prompted results of elevated combustion temperatures as well as a surplus of available oxidizing molecules at stochiometric to fuel-lean O/F ratios. No validation experiments were performed; however, it is posited through the analysis that at an optimal O/F ratio of 16, the upstream burn of gaseous oxygen and gaseous hydrogen would expedite the nylon 6 pyrolysis event and supply enough oxidizer for the pyrolyzed thermoplastic hydrocarbons to sustain a healthy flame. This would promote the heat and mass transfer mechanisms that hybrid rocket propulsion systems are limited to and thus improve regression rates and performance efficiencies.

Acknowledgements

I want to thank my family for their constant love and support throughout all of my life endeavors, especially my academic career.

I want to thank Professor Paul Erickson for giving me an opportunity to conduct research in an area of my passion and providing excellent guidance throughout my graduate degree.

I want to thank Ricardo Gonzalez, Kellen Ochi, Michael Horton, Chibuike Agba, and everyone else in the Energy Research Laboratory at UC Davis for all their help and guidance over the past year and a half.

Nomenclature

γ, Ratio of Specific Heats

r, Function of the Ratio of Specific Heats

σ, Stress, [Pa]

a, Propellant-Characteristic Regression Rate Constant

A, Area, [cm^2]

ABS, Acrylonitrile Butadiene Styrene

AISI, American Iron and Steel Institute

ASA, Acrylonitrile Styrene Acrylate

C^*, Characteristic Exhaust Velocity, [m/s]

C_F, Thrust Coefficient

CAD, Computer-Aided Design

CEA, Chemical Equilibrium with Applications

CO, Carbon Monoxide

CO_2, Carbon Dioxide

ϵ, Expansion Ratio

F, Thrust Force, [N]

FDM, Fused Deposition Modeling

FEA, Finite Element Analysis

G, Total Propellant (Oxidizer and Fuel) Mass Flux Rate, [$kg/m^2 \cdot s$]

g_0, Gravity, [m/s^2]

GH_2, Gaseous Hydrogen

GO_x, Gaseous Oxygen

H_2, Hydrogen

H_2O, Water / Water Vapor

H_2O_2, Hydrogen Peroxide

HTPB, Hydroxyl-Terminated Polybutadiene

h_v, Difference of Heat Content, [J/kg]

I_{sp}, Specific Impulse, [s]

K, Kelvin

L, Length of the Fuel Grain Port, [m]

m, Propellant-Characteristic Regression Rate Constant

M, Mach Number

$\dot{M}$, Mass Flux Rate, [kg/m^2·s]

$\dot{m}$, Mass Flow Rate, [kg/s]

n, Propellant-Characteristic Regression Rate Constant

N, Newton

N_2H_4, Hydrazine

$NaBH_4$, Sodium Borohydride

NASA, National Aeronautics and Space Administration

NH_4NO_3, Ammonium Nitrate

NH_4ClO_4, Ammonium Perchlorate

NO_2, Nitric Oxide

NO_2ClO_4, Nitronium Perchlorate

N_2O, Nitrous Oxide

O_2, Oxygen

O/F, Oxidizer to Fuel Ratio

OH, Hydroxide

p, Pressure, [Pa]

ρ_{fuel}, Fuel Density, [$\mathrm{kg/m^3}$]

P&ID, Piping and Instrument Diagram

PEPU, Polyether Polyurethane

PLA, Polylactic Acid

PP, Polypropylene

PPMA, Polymethyl Methacrylate

$\dot{Q}_w$, Heat Flux Rate, [$\mathrm{J/m^2 \cdot s}$]

R, Gas Constant, [$\mathrm{J/g \cdot K}$]

$\dot{r}$, Fuel Regression Rate, [$\mathrm{m/s}$]

r, Radius, [m]

$\bar{r}_{port}$, Mean Fuel Combustion Chamber Radius, [m]

t, Thickness, [m]

T, Temperature

UC, University of California

u_e, Exhaust Velocity, [$\mathrm{m/s}$]

x, Distance Down Fuel Grain Port, [m]

Chapter 1

Introduction

The global space industry has seen a rebirth of substantial proportions in recent years. With large-scale companies like Blue Origin and Virgin Galactic bringing a rise to the space tourism industry, it is no wonder that over the last decade alone global launch rates have more than doubled [1]. Yet, one facet of the space industry that has seen colossal advancements and is predicted to dramatically grow in the coming decades, is the small satellite industry. Ranging from the miniscule femto scale (0.00 - 0.01 kg) to the mini scale (100 - 180 kg), small satellites are spacecraft that host a wide range of spaced-based instruments intended to advance scientific and human exploration of the Earth and the cosmos. One main contributor to the substantial progress of the small satellite industry over the past two decades has been the development and soaring use of a class of nanosatellites (1 - 10 kg) referred to as CubeSats. Using standard unit dimensions of 10 cm by 10 cm by 10 cm, CubeSats (exemplified in Figure 1.1) are compact, inexpensive, and can perform a variety of scientific investigations and technology demonstrations by utilizing remote sensing [2, 3]. Such functions span from forecasting severe weather patterns on Earth to locating and studying distant exoplanets [4]. However, the true promise of CubeSats is attested by their accessibility to the public for commercial and

educational uses. With a wide range of applicability and advantageous traits, these nanosatellites have flourished in recent years and possess quite a lucrative outlook. In fact, the small satellite industry as a whole is expected to tremendously expand — with market research predicting a multiple billion-dollar growth over the next five years [5, 6]. This provides a great opportunity for smaller, even start-up, companies to engage in providing launch services for these spacecraft.

Figure 1.1. Rendering of Virginia CubeSat Constellation's 'Libertas' satellite [7].

Currently, chemical propulsion systems are the primary technology rockets utilize to deliver payloads, such as individual and constellations of small satellites, into their targeted orbits. Fundamentally, a propulsion system utilizes Newton's second and third laws of motion by accelerating matter to provide a thrust force in order to move a vehicle. In addition to launches, other applications of propulsion systems in regard to space-oriented missions include orbit insertion, orbit maintenance and maneuvering, and altitude control [8]. Chemical propulsion systems — classified by the physical states their propellants (fuel and oxidizer) are stored at — convert energy from chemical reactions (the breaking and forming of chemical bonds) into

kinetic energy. Although liquid and solid propellant propulsion systems have historically dominated large-scale launch missions, hybrid propellant systems have emerged as a prime candidate for smaller operations such as delivering small satellites into low Earth orbit [9]. Hybrid rocket propulsion systems (shown in Figure 1.2) utilize propellants in different physical states and offer numerous advantages over traditional liquid and solid propellant systems. Within the past decade, companies like Vaya Space, HyImpulse Technologies, and BluShift Aerospace (to name a few) have explored and optimized this form of propulsion to fit perfectly as providers for the flourishing small satellite industry [10-12].

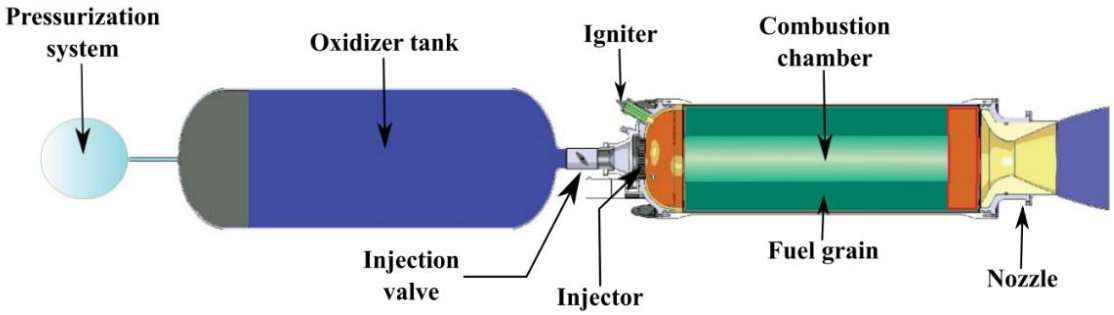

Figure 1.2. Typical hybrid rocket propulsion system anatomy [13].

One area of high concern pertaining to the rise of hybrid rocket propulsion systems as solutions for small scale launch operations is the poor fuel consumption (or regression) rates they experience due to their unique internal ballistics. In a typical hybrid configuration, a liquid or gaseous oxidizer is propelled through a solid fuel grain port where a diffusion-limited combustion process transpires — an event that is highly restricted by heat and mass transfer mechanisms. Due to this circumstance, hybrid rocket propulsion systems have historically and notoriously been characterized as yielding relatively low combustion efficiencies and other performance parameters such as thrust levels [14]. Therefore, it is of utmost importance that

strategies are developed to improve the performance reliability of these propulsion systems in order to meet their growing demand in future small satellite missions.

Chapter 2

Literature Review

In this section, a comprehensive literature review on recent and relevant work is conducted in order to better apprehend where areas of contribution can be made. First, a background in varying chemical propulsion systems is explored — with an emphasis on hybrid rocket technologies. Following is a detailed investigation into current strategies for improving hybrid rocket fuel regression rates. Lastly, a thorough review of hydrogen and nylon 6 as viable propellants is performed.

2.1 Chemical Propulsion Systems

Chemical propulsion systems have historically proved to be the ideal candidate for rocket engines. While nuclear and electric propulsion systems have been tested and theoretically shown to yield high specific impulse values (a parameter of how much thrust is derived from propellant mass flow rate), their limited heritage and low thrust levels have allowed chemical systems — liquids, solids, and hybrids — to become the forefront of the rocket propulsion discussion [8]. All chemical propulsion systems convert energy from chemical reactions — the breaking and forming of chemical bonds — to kinetic energy. Regardless of which of the three physical states

the propellants are in, there are two universal components that all chemical propulsion systems universally share: a combustion chamber, where the heat from the chemical reactions is released, and a converging-diverging nozzle, where the combustion products are expanded out at high velocities to produce useful thrust.

2.1.1 Liquid Propulsion Systems

Liquid propulsion systems, as the name suggests, utilize propellants in liquid physical states. In typical monopropellant systems, a sole liquid substance composed of an oxidizing agent and combustible matter is propelled into a combustion chamber where it is met with a catalyst. The ensuing exothermic chemical reaction produces hot gasses that are expanded out through a nozzle [15]. Typical monopropellants include hydrazine (N_2H_4) and hydrogen peroxide (H_2O_2). Monopropellant systems often yield lower specific impulse values, so they are generally used for orbital insertion and orbital maneuver applications rather than launch missions. Bipropellant systems, on the other hand, feed both a liquid oxidizer and a liquid fuel into a combustion chamber where they react chemically, and their products are similarly exhausted through a nozzle [8]. There are two types of feed systems that are used in order to deliver the propellants to the combustion chamber in bipropellant systems. In tank-pressure fed systems, a high-pressurized, inert gas like helium or nitrogen is introduced to the fuel and oxidizer to propel them forward into the combustion chamber. In pump-pressure fed systems, turbomachinery components — a pump and a pump driver (turbine) — are used to move the propellants. In this turbopump system, an axial inducer is typically placed in front of the pump. The turbine, which rotates both elements by shaft work, is powered by hot gasses from different sources based on which engine cycle design is chosen. There are three primary engine cycles that almost all bipropellant liquid engines utilize. In an expander cycle, high pressure propellant is pumped

through a heat exchanger that is used to cool the thrust chamber structure. Once heated, the propellants are fed into the turbine and, eventually, the combustion chamber. In a gas-generator cycle, a portion of the fuel and oxidizer (typically 2-5%) are pumped through a separate combustor, or pre-burner. These hot combustion gasses are fed into the turbine where they are then exhausted overboard. In a staged-combustion cycle, small amounts of oxidizer feed into the fuel flow, or vice versa, and are directed into a pre-burner. This mixture is partially combusted, producing warm gasses that power the turbine. The partially combusted steam or streams of gasses then enter the main combustion chamber where the combustion process is completed [8]. Oxidizer and fuel combinations can vary greatly for bipropellant systems. Blue Origin, a leader in the liquid rocket engine field, utilizes liquid oxygen and liquid hydrogen for their BE-3 engine [16]. SpaceX, another household name in the liquid propulsion realm, utilizes liquid oxygen and RP-1 for fuel for their Merlin engine [17].

2.1.2 Solid Propulsion Systems

Solid propellant propulsion systems utilize solid fuel grains that contain both an oxidizer and a fuel component in its composition. There are two general categories for solid propellants: double base and composite. Double base propellants form a homogenous fuel grain where both the primary ingredients — usually a nitrocellulose type of gun powder dissolved in nitroglycerine — contain fuel and oxidizer [8, 15]. Although double base propellants have historically seen use in military applications such as ballistic missiles, they have fallen in popularity to composite propellants. Composite propellants are constructed of a heterogenous mixture of oxidizer, fuel, and binder. The oxidizers in these types of propellants are typically crystalline compounds with high oxygen content. Commonly used oxidizers include ammonium nitrate (NH_4NO_3), ammonium perchlorate (NH_4ClO_4), and nitronium perchlorate (NO_2ClO_4). The fuels used in

composite propellants are typically metallic powders such as titanium, magnesium, or aluminum (the most common). Binders, or the substances that hold the complete formulations together, are commonly long-chained polymers like polyether polyurethane (PEPU) or the popular hydroxyl-terminated polybutadiene (HTPB). With the addition of a curing agent and high temperature heating, cross-linking is promoted, and the polymer hardens the entire propellant grain [8, 15]. This propellant grain is constructed into a unique port configuration, dependent on a desired thrust profile, and fitted into a high strength motor case. This port, or "bore", travels from the entrance of the motor case, where a pyrogen igniter sits, to the nozzle where the combustion gasses are expanded out at high speeds.

Although solid propellant propulsion systems have been utilized in military applications such as ballistic missiles, they are often employed as first-stage boosters for space-launch vehicles due to the high thrust levels that they can produce. They have also seen implementation in upper stage and orbital-transfer vehicles [8]. Additional advantages of solid propellant propulsion systems include overall system simplicity as well as the ability to maintain a compact size due to the high-density propellants which require less storage volume. Specific impulse values for these systems, however, are generally lower due to less chemical bond energy in the propellants themselves. Thrust cannot be manipulated either in solid propellant propulsion systems. Once ignited, similar to a firework, the grain burns until there is no more propellant left for combustion. However, one of the most significant drawbacks of solid propellant propulsion systems is the hazardous exhaust that many fuel and oxidizer combinations can produce. The most common oxidizer for solid propellant rockets, ammonium perchlorate, can produce exhaust that is up to 14% hydrochloric acid — a toxic gas that can contribute to acid rain and stratospheric ozone depletion [8, 15]. Beryllium, an energetic choice for solid propellant fuel,

yields beryllium oxides during combustion. Exposure to this compound, generally through inhalation, can lead to a form of metal poisoning called berylliosis — a complication with lung afflictions similar to long-term asbestos exposure. Yet, there are still numerous other oxidizer, fuel, and binder combinations that designers can pick from that will yield cleaner combustion products.

2.1.3 Hybrid Propulsion Systems

A hybrid rocket propulsion system utilizes propellants in two different physical states — liquid (or gas) and solid. A launch vehicle that employs this type of chemical propulsion system is referred to as a hybrid rocket. Classical hybrid rockets consist of a liquid oxidizer that is propelled through a solid fuel grain. Although it is possible to manufacture a "reverse hybrid" with liquid fuels and solid oxidizers, the concept is uncommon in literature and industry [8]. Hybrid rocket technology dates back to late 1930's Germany, where efforts by I.G. Farben were first attempted in utilizing coal and gaseous nitrous oxide for propellants. Over the following decades, investigations from institutions such as the California Pacific Rocket Society and United Technologies Center established the traditional propellant combinations seen today like liquid oxygen and various polymers. More recent research has extended the scope into characterizing the specific combustion processes and internal ballistics that are unique to hybrids [8].

Hybrid rockets, almost exclusively, utilize carbon-based polymers for their solid fuel source [8]. These polymers, or macromolecules composed of bonded subunits (monomers), can be further divided into thermoplastics and thermosets. Upon heating, thermoplastics soften and can be reshaped with heat and pressure. Thermosets, conversely, are polymers that cannot be softened or reshaped upon reheating [18]. In hybrid rocket applications, these polymers are

almost always in the form of plastic or rubber. Due to significant manufacturing advancements such as rapid prototyping, hybrid rocket fuel grains have become remarkably easier to produce. Fused deposition modeling (FDM), or 3D printing, has paved the way for engineers to overcome manufacturing limitations by allowing them to use a wide variety of materials and geometric configurations for their fuel grain designs. With thermoplastics largely dominating the landscape of hybrid rocket fuels for multiple decades, this manufacturing method has proved incredibly beneficial in producing conventional fuel grain candidates such as acrylonitrile butadiene styrene (ABS), acrylonitrile styrene acrylate (ASA), and polymethyl methacrylate (PMMA) [19]. Alternately, one of the most popular fuel selections in the history of hybrid rockets is the thermosetting HTPB. Beginning as a liquid resin, this rubbery compound is manufactured by being poured into a mold and cured to a stiff material with the addition of a hardener [20]. Energetic, readily available, and very safe to handle, HTPB is such a commercially viable option that it is even utilized as the fuel grain material for Virgin Galactic's SpaceShipTwo hybrid propulsion system, as seen in Figure 2.1 [8, 21].

Figure 2.1. Virgin Galactic's RocketMotorTwo abord SpaceShipTwo [21].

Two of the most popular oxidizers used for hybrid rockets in recent literature have been oxygen (O_2) and nitrous oxide (N_2O) — either in a liquid or gaseous phase. Liquid oxidizers provide higher volumetric energy densities than gasses do, so they are typically used more frequently for performance-critical projects or where the use of smaller tanks are crucial to mass requirements. However, certain care must be taken when handling liquid oxidizers (such as the widely used oxygen) as their extremely low temperatures classify them as cryogenics. Virgin Galactic has historically employed liquid nitrous oxidizer for their hybrid rocket designs, including RocketMotorOne and RocketMotorTwo [21]. Liquid hydrogen peroxide (H_2O_2) has also seen significant utilization as an oxidizer in hybrid propulsion systems [22]. However, it is generally difficult to ignite and is typically unable to perform dependable cold starts [23]. Gaseous oxidizers, on the other hand, are typically safer to handle and store, so they are frequently used in experiments across academia.

Due to differing propellant physical states, hybrid rocket combustion is quite distinct and varies from that of both liquid and solid rockets. Whether the oxidizer is directly injected as a gas or is first propelled as a liquid and atomized through an injector plate, the combustion event that occurs once ignition begins is akin to that of a turbulent diffusion flame [8]. A diffusion flame occurs in a realm where an appropriate concentration of initially separated fuel and oxidizer come together, through molecular and turbulent diffusion, and allows for combustion [24]. In hybrid rockets, this flame is established within the boundary layer — a region of flow near the solid fuel grain surface that experiences lower flow velocity due to viscous shear forces between the oxidizer stream and the grain surface itself [8]. As shown in Figure 2.2, the vaporized fuel — deriving from the pyrolysis of the fuel grain — enters into the boundary layer and meets with the

free-stream oxidizer (transported by turbulent diffusion) at the flame zone [15]. Thus, hybrid rocket combustion is characterized as a diffusion limited process.

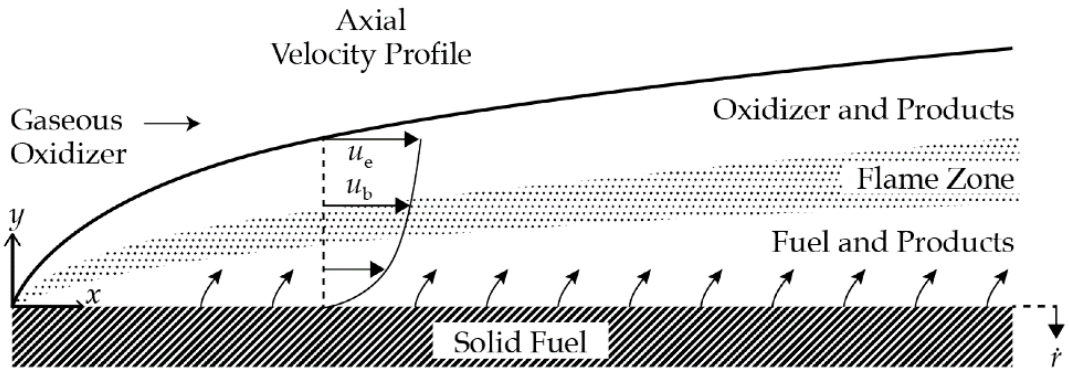

Figure 2.2. Hybrid Rocket diffusion-limited combustion process [25].

The heat transferred from the flame to the fuel grain surface in a steady state operation is identified by Equation 2.1 [8]:

$$\dot{Q}_w = \dot{M}_f \, h_v \tag{2.1}$$

where $\dot{Q}_w$ is the heat flux rate [J/m^2·s], $\dot{M}_f$ is the mass flux rate of vaporized fuel (perpendicular to the solid grain surface) [kg/m^2·s], and h_v is the difference of heat content between a unit mass of gasified fuel at the surface and the heat content of the solid fuel at ambient temperature [J/kg]. The h_v parameter includes the heat to warm the solid to the surface temperature, thermal changes prior to gasification (like depolymerization), and the heat of vaporization. The performance of hybrid rockets is dictated by fuel regression rate (the rate of solid fuel consumption). Formulas to express this phenomenon are largely empirically derived. The renowned general model within theory is shown in Equation 2.2 [8, 26, 27]:

$$\dot{r} = a \, G^n \, x^m \tag{2.2}$$

where $\dot{r}$ is the overall fuel regression rate [m/s], G is the total propellant (oxidizer and fuel) mass flux rate [kg/m^2·s], x is the distance down the port [m], and a, n, and m are propellant-

characteristic regression rate constants. However, time-averaged formulas have also been derived that reduce complexity for calculating these rates, as shown in Equation 2.3 [19]:

$$\bar{\dot{r}} = \frac{\dot{m}_{fuel}}{\rho_{fuel} \cdot 2 \cdot \pi \cdot \bar{r}_{port} \cdot L} \tag{2.3}$$

where $\dot{m}_{fuel}$ is the time-average mass flow of the fuel [kg/s], ρ_{fuel} is the fuel density [kg/m^3], $\bar{r}_{port}$ is the mean fuel combustion chamber radius [m], and L is the length of the fuel grain port [m].

To initialize the fuel grain pyrolysis event, different ignition methods for hybrid rockets have been utilized across academia and industry. Pyrotechnic ignition is a very common method in the hybrid rocket world due to its simplicity and reliability. Acting as a small solid rocket motor itself, a pyrotechnic igniter uses an electronic match (or squib) to heat a solid grain of premixed oxidizer and fuel. This small ignition event then initiates the combustion of the larger fuel grain of the rocket [28]. The drawback of this method is that pyrotechnics are generally only available for single ignition events, making it a poor choice to exemplify a hybrid's restart capabilities. In hypergolic ignition, a spontaneous combustion process starts when two particular propellants come into direct contact with each other. A way to achieve hypergolic ignition in hybrid rockets is to embed catalyst particles within the hydrocarbon fuel grain that initiate combustion on direct contact with a specific oxidizer. One such example of this method is embedding polyethylene fuel grains with sodium borohydride ($NaBH_4$) catalyst, which spontaneously combusts when coming into contact with H_2O_2 — a popular oxidizer in the hybrid rocket world [29]. Novel solutions to ignition have also been developed. A low power arc-ignition system created by Utah State University utilizes electrodes that are embedded into the fuel grain as a region of electrostatic potential. Due to the unique electrical breakdown properties that polymers like ABS experience when manufactured using FDM, the electrostatic

region causes an inductive arc and initiates pyrolysis of the fuel grain [23]. Yet, one of the most promising forms of ignition for hybrid rockets is the hydrogen-oxygen torch. In this ignition system, gaseous hydrogen and gaseous oxygen are individually flown into a general injector assembly where a spark plug ignites the mixture before propelling down the fuel grain. The NASA Lewis Research Center has demonstrated this method to be incredibly reliable — firing the torch up to 400 times before needing replacement. One of the strongest key factors of this ignition system is its ability to produce extremely fuel-lean flames up to 40 O/F, due to the properties of hydrogen-oxygen combustion. This results in a relatively low combustion temperature, and thus eliminates the need to externally cool the ignition combustion chamber [30]. This torch ignition method has also been thoroughly explored and tested utilizing methane as the fuel source [31, 32].

Hybrid rockets exhibit numerous advantages over traditional liquid and solid propellant systems. Due to the solid fuel grain remaining inert until ignition and stored entirely separate in a different phase from the oxidizer, hybrids are quite safer than their chemical propulsion counterparts. This zero TNT equivalence, alongside the insensitivity of cracks and defects in the fuel grain during combustion, makes hybrids an attractive option [33]. Unlike solid rockets, hybrids have re-start capabilities and can be throttled by controlling the amount of oxidizer that is flown into the fuel grain. This widens their applicability into precise missions such as orbit maneuvers. Additionally, due to the rise of rapid prototyping techniques such as FDM, hybrid fuel grains can be manufactured at a high rate — lowering overall system costs [19]. These system costs are further reduced, in comparison with liquid and solid rockets, from their simpler handling and storage requirements. Environmentally, hybrids have a large range of available propellant combinations that can stray away from undesirable combustion products [8]. This

allows the use of “green” alternatives for propellant options [23]. Although typically falling in between its fellow chemical systems in regard to performance parameters, hybrids have been proven to meet the capabilities of some liquid propellant combinations such as liquid oxygen and RP-1 [25]. The ultimate design simplicity of hybrids — attributed to the reduced number of system components — also boosts their practicality for mission applications [15].

Although showcasing many superior traits, there are a few disadvantageous features that hybrids are notorious for in the propulsion realm. One significant drawback is the oxidizer to fuel (O/F) ratio shift that is experienced during combustion [34]. Due to the fuel grain regression, the surface area of the internal port increases with time at a constant oxidizer mass flow rate. This is exacerbated if the oxidizer is throttled. This, in turn, causes an overall proportion variance from the initial O/F ratio due to the consumption of more fuel over time. Accordingly, this varies the thrust levels and specific impulse values derived during firing as well [8]. Due to the use of fluid oxidizers, hybrids also possess lower density-specific impulses than that of solid propellant rockets [15]. Yet, the most prominent drawback that hybrids demonstrate is low fuel regression rate, which correlates to lower performance levels. The pyrolysis event that the solid fuel grain experiences is limited by the heat transfer supplied by the diffusion flame. This heat must be enough to liberate the solid molecules from the grain to a gaseous phase that can enter the overall flow stream. A proper ignition method then must provide the required activation energy to begin the burn. During combustion, however, there is relatively poor propellant mixing within the boundary layer. This low degree of mixing translates into lower combustion efficiencies [14]. Each of these drawbacks, however, has seen serious mitigation efforts — keeping hybrids as promising options not only for small launch systems, but upper stage, lunar, and even Mars ascent stage vehicles [35].

2.2 Fuel Regression Enhancement Strategies

A wide array of investigations have been performed in identifying methods to improve fuel grain regression rates for hybrid rocket propulsion systems. These studies have largely focused on techniques of increasing the heat transfer from the combustion zone within the boundary layer to the surface of the fuel grain [36]. Novel techniques of magnifying mass transfer mechanisms have also been explored.

2.2.1 Port Configuration

One area of high experimentation for regression enhancement is fuel grain port geometry and configuration. Beyond single, centered bores, port configuration complexity can range anywhere from wagon wheel orientations to the effective seven-cylinder cluster design — the former of which can provide enhanced fuel volumetric efficiencies (volume of the fuel / volume of the chamber) [8]. Incentivized by the rise of fused-deposition modeling techniques as a rapid and robust manufacturing method to produce complex fuel grains, designers have investigated these multiple-port patterns in an attempt to increase surface burn area [37]. This can translate into higher fuel mass flow rates and ultimately better performance parameters such as thrust and specific impulse. Experiments have shown that the use of these multi-port geometric configurations (such as shown in Figure 2.3) can produce higher regression rates than that of single ports alone [38].

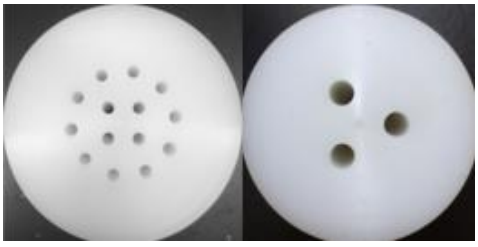

Figure 2.3. Multi-port patterns for hybrid rocket fuel grains [39].

Helical port structures have also been identified as significantly improving regression rates as well as keeping adequate volumetric efficiencies [37, 40, 41]. This can be attributed to a rise in the convective heat transfer derived from the centrifugal forces compressing the boundary layer further near the fuel grain wall. Yet, one major drawback of using any geometrically complex configuration is the potential for uneven port burning and eventual reduced fuel grain integrity [37]. Although web supports made from slow-burning plastic materials can be implemented to combat this structural degradation, designers still must optimize their fuel grain configurations for rigidity during the latter half of the combustion process [8].

2.2.2 Liquifying Fuel Grains

Another solution that has been identified for improving hybrid rocket regression rates is the utilization of liquefying fuel grains. These types of fuels are characterized as having low enthalpy of vaporization values and promoting a mass-transfer mechanism during combustion due to the entrainment of liquid droplets into the overall flow stream [33]. This stems from a hydro-dynamically unstable melt layer that arises from the fuel grain burning surface, as shown in Figure 2.4 [42].

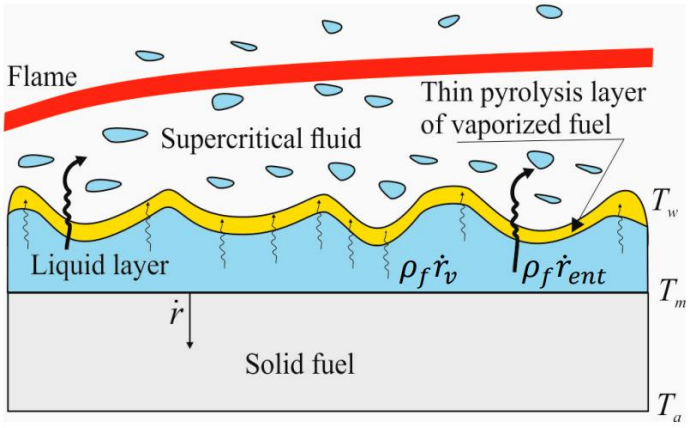

Figure 2.4. Unstable melt layer for liquifying fuels [43].

Paraffin wax has dominated recent literature as a prime liquifying fuel choice for hybrid rocket applications. Although a wide array of formulations exists, one typical source that has seen much experimentation is SasolWax 0907 ($C_{50}H_{102}$). This brittle microcrystalline wax's traditional utilization originates in cosmetic-oriented products ranging from lip balm to creams and lotions [44]. Yet, when manufactured using a popular die casting method, a homogenous fuel grain can be formed for combustion uses [42]. One fuel blend of paraffin waxes — including SasolWax 0907 — has even been scaled up to a 1000 N breadboard system and exemplified stable combustion during testing [34]. However, one major drawback of paraffin waxes and liquefying fuels in general are their inherent structural deficiencies. Paraffin-based fuel blends typically exhibit mechanical properties that are significantly weaker than classical thermoplastic polymers. For example, W1 — a paraffin fuel blend composed of 99% SasolWax 0907 and 1% carbon powder — demonstrates a compressive yield strength of only 3.46 MPa compared to PLA (polylactic acid), which exhibits a 68.48 MPa compressive yield strength under similar testing environments [45]. Due to this drawback, liquefying fuel grains are generally utilized with other supporting reinforcements, like self-disintegrating skeleton structures or metal additives [46].

2.2.3 Metal-Based Energetic Additives

Metal-based energetic additives have undergone thorough experimentation in recent years as a valid regression enhancing tool for thermoplastic and thermosetting polymers. The goal of supplementing metal into the fuel grain is to enhance the flame temperature and subsequent radiative heat transfer during combustion of the rocket. This promotes faster regression rates and higher fuel mass flow rates. Recent lab-scale firing investigations showed that micro to nano sized aluminum-based fillers increased regression rates by 54% and fuel mass burning rates (flow rates) by 141% when combined with HTPB in a composite formulation compared to HTPB

alone at equivalent oxidizer flow rates [47]. Another prominent study from recent literature showed that the use of one-micrometer magnesium particles in a paraffin fuel (accounting for 15% mass of the total solid grain) improved regression rates by 163.2% compared to baselines without it [33]. In fact, aside from performance enhancement, metal additives have seen great implementation as structural rigidity supplements — such as the use of aluminum particles to increase ultimate tensile strengths of liquifying fuels [46]. Yet, one drawback of using metal-based energetic additives for regression enhancement is that they have shown to sometimes produce high amplitude, low frequency pressure oscillations [48]. This is not ideal when trying to retain a stable combustion process during rocket firing.

2.2.4 Swirl Injection

Swirl injectors have also been examined as an application for increasing fuel grain regression rates. The utilization of this method amplifies the turbulence intensity of the oxidizer within the fuel grain. Once ignited, the shear effect of heat flow on the fuel grain surface is enhanced, thus promoting the heat flux density at the boundary layer and overall heat transfer during the combustion process [49]. VH-20, a hybrid rocket system utilizing a coaxial, co-swirling, counterflowing vortex pair, was shown to yield regression rates up to seven times faster than traditional hybrid injection methods. As shown in Figure 2.5, this configuration propels oxygen through a swirl injector near the converging entrance of the nozzle. The vortex that is created swirls upward along the port surface, mixing with the pyrolyzed fuel. It then turns inward at the front of the fuel grain and spirals back down toward the nozzle [50].

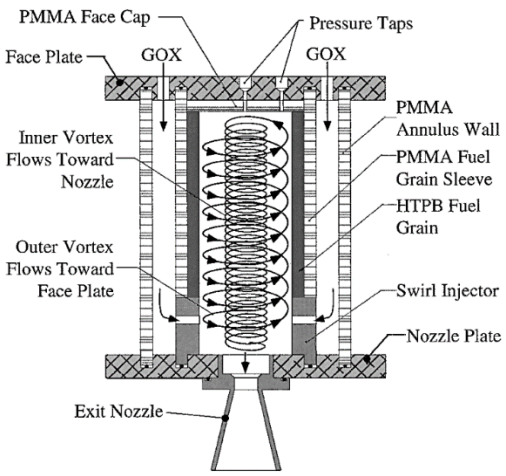

Figure 2.5. VH-20 swirl injection system diagram [50].

Configurations with the swirl injector at the head of the fuel grain have also been tested and shown to increase regression rates from that produced by linear oxidizer injection [51]. Swirl injection has also seen implementation with helical fuel port structures, showing that a suitable combination of the two strategies can also enhance fuel consumption rates [52]. Multi-section swirl injection has also proven to yield higher regression rates than conventional linear injection methods [53]. However, one major disadvantage this enhancement strategy possesses as a whole is the labor time and effort required to set up the testing environment. This spans from the complicated piping systems that are required to the distinct machining typically necessary for the injector blocks or combustion chambers.

2.2.5 Hydrogen Co-firing

One potential fuel regression enhancement technique that has been explored by the Energy Research Laboratory at the University of California, Davis is the use of hydrogen as a supplemental propellant to a standard hybrid rocket propulsion system of gaseous oxygen and ABS thermoplastic fuel grain. Hydrogen enrichment has seen significant experimentation in recent years with internal combustion engines and has been implemented as an additive in a wide

variety of fuels including ethanol, compressed natural gas, landfill gas (largely methane), and gasoline. In the past, this fuel enhancement method has shown to reduce adverse emissions such as NO_2 (nitric oxide) in applications such as two-cylinder, spark ignition engines [54, 55]. Previous studies using gasoline Wankel rotary engines for this fuel enrichment strategy also demonstrated increased fuel economy, improved thermal efficiency and engine stability, higher power output, as well as a reduction in unfavorable combustion products such as carbon monoxide and hydrocarbons [56, 57]. In addition to validating the use of a hydrogen-oxygen torch igniter as a hybrid rocket ignition system, experiments run by the UC Davis Energy Research Laboratory showcased an increase in average linear regression rates of ABS during static firings for stoichiometric to fuel-lean O/F ratios of hydrogen and oxygen [58]. Although this technique is quite novel in academia, it shows promising initial results for further experimentation and validation in hybrid rocket applications.

2.3 Hydrogen

Consisting of just one proton and one electron, hydrogen is the simplest, lightest, and most abundant element in the known universe. On Earth, hydrogen naturally exists as a diatomic molecule, H_2, most prominently conjoined with oxygen to form water (H_2O). It is also abundantly found linked with other elements to form organic compounds such as hydrocarbons. Below its incredibly low boiling point of 20 K (-423 F), hydrogen exists as a liquid [59]. Typically, it is only found in this physical state when being utilized for cryogenic applications, such as fuel for liquid propulsion systems. In fact, hydrogen has seen a long track record of implementation in liquid propellant rockets — from the historic Aerojet Rocketdyne RS-25 (Space Shuttle Main Engine) to the more recent Blue Origin BE-3 engine. There are multiple ways that hydrogen can be produced, but the two most popular methods are electrolysis and

steam-methane reformation [60]. In the carbon-free production process of electrolysis, electricity is used to split water into its constituents of oxygen and hydrogen. Alternatively, steam-methane reformation involves the utilization of a catalyst to induce a chemical reaction between natural gas (primarily methane) and water to yield hydrogen [61].

Hydrogen exhibits numerous unique combustive properties, which makes it an interesting candidate for combustion and propulsion applications. One of the most advantageous traits it exhibits is an incredibly wide range of flammability. The flammability limits of hydrogen in oxygen (for rocket applications) are approximately 4 to 94% [24, 62]. This opens up a plethora of possible O/F ratios that can produce a successful ignition event. Hydrogen also possesses low ignition energy — making it easily ignitable and a prime candidate for lean mixtures. As shown in Figure 2.6, the flame speeds that hydrogen produces at stoichiometric conditions are orders of magnitude greater than that of other fuels [59].

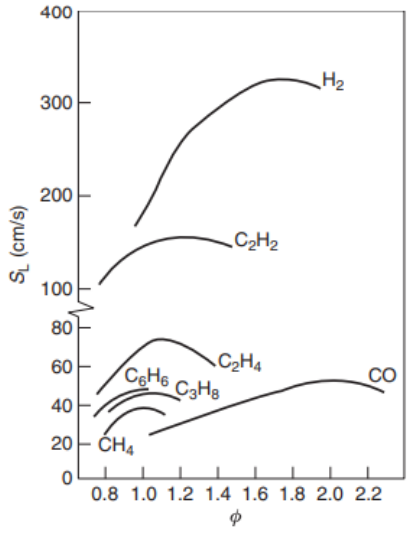

Figure 2.6. Laminar flame speeds as a function of equivalence ratio Ø for various fuel-air combinations [24].

The high diffusivity of hydrogen can also facilitate better propellant mixing and increased heat transfer. Additionally, when hydrogen is combusted with oxygen, the products are largely water vapor. This makes hydrogen a more environmentally friendly fuel than other hydrocarbons that produce CO_2, CO, and NO_2 [63]. Hydrogen has a staggering specific energy (energy per mass) content of approximately 120 MJ/kg — roughly three times that of gasoline and more than double that of methane. Conversely, gaseous hydrogen has a disadvantageous energy density (energy per volume) of approximately 2 MJ/L when compressed at 5,076.32 psi (350 bar) and 8 MJ/L when in a liquid state [64]. This generally translates into the use of larger tanks in order to achieve the same energy content per volume as other fuels. This, in turn, increases the inert mass (the mass of the rocket without propellant or a payload) of the overall rocket, which can be detrimental to mission criteria. However, despite this drawback, the promising traits that hydrogen demonstrates makes it a promising augmenter of heat and mass transfer — and ultimately regression rates — when used in a torch igniter configuration for hybrid rocket propulsion systems.

2.4 Nylon 6

Nylon fuels have been relatively unexplored in the hybrid rocket field, especially compared to other thermoplastics such as ABS and PMMA. Their uses in the hybrid propulsion realm have been largely limited to structural reinforcement. Armored paraffin grains hosting printed nylon cellular structures have demonstrated successful mechanical enhancement, including a 35% increase in yield strength and 296% increase in yield strain compared to pure paraffin grains [45, 65]. Larger skeleton structures and protrusion mechanisms are other applications that have been explored with nylon thermoplastics [66, 67]. However, the limited literature that does exist on its combustion properties shows that it could be a very favorable family of polymers to explore for

fuel grain purposes. One prominent study of various thermoplastic fuels showed that nylon — alongside ASA — produced the highest regression rates of all other tested candidates during firing. The polymer outperformed popular fuel grain candidates such as ABS, PP (polypropylene), PLA, and even a composite formulation of PLA with aluminum metal additives [19]. This provides a strong justification for further testing and cross comparison to other thermoplastics.

Nylon 6, one formulation within the family of synthetic polymers, shows to be an easily accessible, manufacturable, and mechanically superior candidate for hybrid rocket applications. In recent years, nylon 6 has seen extensive use as a premier material within the automotive industry for applications such as engine covers and fuel filter lids. Additionally, this polymer has experienced utilization as material for mechanical gears, machine guards, and even toothbrush bristles. This thermoplastic is constructed by the polymerization of caprolactam — a monomer hosting 6 carbons (hence nylon "6") [68]. With a chemical formula of $(C_6H_{11}NO)_n$, nylon 6 yields a molecular mass of 113.16 g/mol. One formulation of the polymer created by Mitsubishi Chemical Advanced Materials (reflective other formulations) hosts an ultimate tensile strength of 88 MPa — more than double that of many blends of the popular thermoplastic, ABS [69, 70]. Alongside favorable stiffness and hardness properties, as well as a relatively low melting temperature of 488.15 K (215 C), nylon 6 presents itself as a prime candidate for hybrid rocket propulsion applications [69].

Chapter 3

Theoretical Approach

This body of work seeks to design, manufacture, and perform simulated performance analysis on an operation-ready hybrid rocket propulsion system of gaseous oxygen and nylon 6 thermoplastic fuel grain with a hydrogen co-firing configuration. This will provide a platform and scientific basis for investigations into further validating the regression and performance-enhancing properties that hydrogen has shown to possess at stochiometric to fuel-lean O/F ratios. This will additionally provide a premise to further uphold the practicality of the oxygen-hydrogen torch ignition system with a novel thermoplastic fuel grain candidate for hybrid rocket applications. In this chapter, an entire theoretical system is calculated with performance parameters for initial assessment and post-simulation efficiency calculations.

3.1 Overview

The theoretical hybrid rocket propulsion system was designed around an existing static fire fixture at the University of California, Davis's Energy Research Laboratory and was the basis for all theoretical calculations — providing the boundary conditions for all other system components. This fixture consists of three main elements: an injector block (for the use of a

hydrogen-oxygen torch ignition system), a combustion chamber cylinder, and a post-chamber structural block. A computer-aided design model is seen below in Figure 3.1.

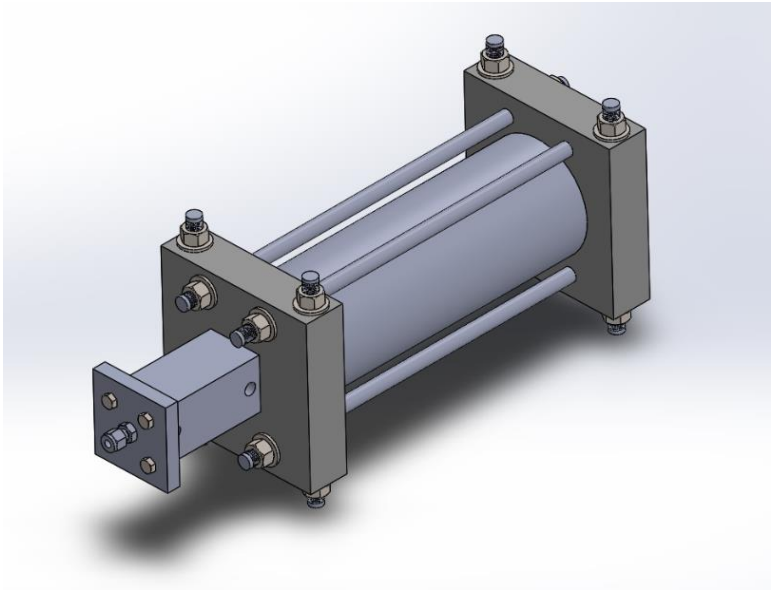

Figure 3.1. CAD model of static fire fixture [58].

3.2 Assumptions

To appropriately design the propulsion system, a few assumptions were made to reduce calculation complexity. First, the entire system was treated at a steady state condition, with no variables changing with time. The system was also assumed to be well insulated, and that the injector block, combustion chamber cylinder, and post-chamber structural block were all adiabatic. It was deduced from a manufacturing standpoint that a converging-diverging conical nozzle would be designed, and that gaseous oxygen was to be the propellant at the nozzle throat. This was due to a lack of existing literature on the pyrolysis event that nylon 6 experiences during combustion, including heat of gasification values. Therefore, the H_2/O_2 burn was considered for combustion products utilizing NASA CEA (Chemical Equilibrium with Applications) code [71]. At the desired time intervals of flow and fuel-lean O/F ratios initially

assessed, the substantial product was computed to be oxygen. This propellant was treated as a quasi-one-dimensional flow and as an ideal gas with a constant ratio of specific heats (γ=1.4 for diatomic gases). It was assumed that at the throat of the converging-diverging nozzle the flow would be choked, thus yielding a Mach number equal to 1. Additionally, the combustion chamber temperature during firing was assumed to be 3000 K — another result derived from the H_2/O_2 CEA simulation.

3.3 Theoretical Design

The propulsion system was designed utilizing three independent variables: nozzle exit pressure, stagnation chamber pressure, and nozzle throat area. A presumption was made that the ambient pressure surrounding the system was directly equal to the exit pressure of the nozzle, thus operating at maximum thrust. Therefore, the nozzle exit pressure was identified as 101.353 kPa (14.7 psia). Lab limitations at the University of California, Davis's Energy Research Laboratory determined the stagnation chamber pressure. Based on available pressure regulators for K size tanks of oxygen and hydrogen, a chamber pressure of 1.034 MPa (150 psia) was decided to cope with pressure loss in the fluid lines. With this pressure ratio in mind, the flow through the nozzle was first examined. An exit Mach number was calculated utilizing an isentropic relationship, Equation 3.1 [8], for compressible flow:

$$\frac{p_e}{p_c} = (1 + \frac{\gamma-1}{2} {M_e}^2)^{\frac{\gamma}{\gamma-1}} \tag{3.1}$$

where p_e is the nozzle exit pressure [Pa], p_c is the chamber pressure [Pa], γ is the ratio of specific heats for oxygen, and M_e is the Mach number at the nozzle exit. The given pressure values yielded a Mach number at the nozzle exit of 2.17. This value was then used to determine the nozzle expansion ratio (ϵ) by applying Equation 3.2 [8]:

$$\epsilon = \frac{A_e}{A_t} = \frac{1}{M_e}\sqrt{\left[\left(\frac{2}{\gamma+1}\right)\left(1+\frac{\gamma-1}{2}{M_e}^2\right)\right]^{\left(\frac{\gamma+1}{\gamma-1}\right)}} \quad (3.2)$$

where A_e is the cross-sectional area of the nozzle exit [cm^2] and A_t is the cross-sectional area of the nozzle at the throat [cm^2]. This relationship yielded an expansion ratio — from the nozzle throat to the nozzle exit — of 1.95. The next design step was to identify either a nozzle throat diameter or nozzle exit diameter. With a known expansion ratio, one value would derive the other. The nozzle throat diameter was chosen to be .762 cm (.3 in) for manufacturing ease — yielding a nozzle throat area of .456 cm^2 (.0707 in^2). Using Equation 3.3:

$$A_e = \epsilon \cdot A_t \quad (3.3)$$

the nozzle exit area was calculated as .89 cm^2 (.138 in^2) and a nozzle exit diameter of 1.064 cm (.419 in). With the pertinent nozzle geometry completed, the next design step was to identify the maximum mass flow rate at the throat. This was accomplished by utilizing Equation 3.4 [8]:

$$\dot{m}_{t(max)} = \frac{A_t p_c}{\sqrt{\gamma R T_c}}\Gamma \qquad \Gamma = \gamma\left(\frac{2}{\gamma+1}\right)^{\frac{\gamma+1}{2(\gamma-1)}} \quad (3.4)$$

where $\dot{m}_{t(max)}$ is the maximum mass flow rate at the throat [g/s], R is the gas constant for oxygen [J/g·K], T_c is the stagnation chamber temperature [K], and Γ is a function of the ratio of specific heats (γ). This yielded a maximum propellant mass flow rate at the nozzle throat of 36.58 g/s. This value was key in computing the first major performance parameter of the rocket propulsion system as shown in Equation 3.5 [8]:

$$C^* = \frac{A_t p_c}{\dot{m}_t} \quad (3.5)$$

where C^* is the theoretical characteristic exhaust velocity [m/s]. This value characterizes the propellant and chamber performance of the rocket independent of the nozzle. This parameter is

key in computing the combustion efficiency of the physical rocket design and is universally implemented in propulsion systems engineering to assess propellant and chamber performance. The characteristic exhaust velocity of the theoretical design was calculated to be 1289.3 m/s (2884.08 mph). The next performance parameter that was solved is displayed in Equation 3.6 [8]:

$$u_e = \sqrt{\frac{2\gamma RT_c}{\gamma-1}\left[1-\left(\frac{p_e}{p_c}\right)^{\frac{\gamma-1}{\gamma}}\right]} = \sqrt{\frac{2\gamma RT_c}{\gamma-1}\left[1-\left(1+\frac{\gamma-1}{2}{M_e}^2\right)^{-1}\right]} \tag{3.6}$$

where u_e is the exhaust velocity of the rocket's gasses [m/s]. Either method of calculation could have been utilized due to the isentropic relationships of compressible flow. Exhaust velocity is a key component in the ideal (or 'Tsiolkovsky') rocket equation and is critical for mission planning. This value was found to be 1626.7 m/s (3638.82 mph) — reasonably higher than the characteristic exhaust velocity. With a true exhaust velocity and mass flow rate computed, an overall thrust force [N] could be calculated by the simple formula, Equation 3.7:

$$F = \dot{m}_t \cdot u_e \tag{3.7}$$

This relationship yielded a theoretical maximum thrust force of 59.5 N (13.37 lbf) — well in line with other hybrid rocket propulsion system designs throughout academia [72-74]. In order to identify how efficiently the energy content from the propellants is converted into useful thrust force, another performance parameter was computed, as seen in Equation 3.8 [8]:

$$I_{sp} = \frac{F}{\dot{m}_t\, g_0} \tag{3.8}$$

where I_{sp} is the specific impulse of the rocket [s] and g_0 is gravity [9.807 m/s^2]. Specific impulse is universally used in the rocket industry to identify overall engine efficiency. The

theoretical specific impulse found for this system design was 165.8 s. Lastly, a final performance parameter (Equation 3.9 [8]) could be calculated to identify how efficiently the nozzle design amplifies the overall thrust force:

$$C_F = \frac{F}{A_t p_c} \tag{3.9}$$

where C_F is the dimensionless coefficient of thrust. This was calculated to be 1.261 for the theoretical system.

With theoretical performance parameters found, the next design move was to breakdown the maximum fluid mass flow rate at the nozzle throat into individual propellant mass flow rates. One previous study utilizing ABS with a hydrogen co-firing configuration showed that stochiometric and fuel-lean ratios of fuel and oxidizer were advantageous to improving fuel consumption rates over fuel-rich ratios. Within this study, one experimental run within the design matrix yielded a maximum, time-average thermoplastic regression rate that accounted for approximately 35.15% of the overall mass flow rate during firing. Due to no existing pyrolysis or regression data found in literature for nylon 6, this value was utilized to approximate a realistic amount of thermoplastic fuel that would be introduced into the overall propellant flow stream during combustion. This resulted in a nylon 6 time-average mass flow rate approximation of 12.86 g/s. Using a basic mass conservation breakdown, as seen in Equation 3.10, the remaining 23.72 g/s of propellant would be split between hydrogen and oxygen at a desired O/F ratio.

$$\dot{m}_{t(max)} = \dot{m}_{O_2} + \dot{m}_{H_2} + \dot{m}_{nylon\,6} \tag{3.10}$$

For this theoretical design, it was decided an O/F ratio of 16 would be targeted to further elucidate the effects of a fuel-lean operation. This would allow studies to vary hydrogen flow time at a fixed rate to identify regression and performance results. Thus, an oxygen mass flow

rate of 22.325 g/s and a hydrogen mass flow rate of 1.395 g/s was confirmed for the physical rocket configuration.

Chapter 4

Manufacturing Approach

4.1 Rocket Propulsion System Design

An entire hybrid rocket propulsion system with a hydrogen co-firing configuration was constructed for the intended utilization within studies to elucidate the possible regression-enhancing properties that hydrogen can posses when used as a supplemental propellant. This chapter details the construction of all subsystems for the physical design.

4.1.1 Static Fire Fixture Design and Test Stand

The first component of the hybrid rocket propulsion system was the existing static fire fixture at the University of California, Davis's Energy Research Laboratory. The injector block was constructed out of AISI 304 stainless steel and hosts an inlet for gaseous oxygen, gaseous hydrogen, a pressure transducer, and a Bosch Iridium spark plug. As shown in Figure 4.1, the gaseous oxygen stream flows axially down the injector port whereas the hydrogen flow enters in the radial direction. This was originally constructed to minimize swirl injection and force the hydrogen to converge into the overall propellant stream. The pressure transducer was placed

after the spark plug and close to the main combustion chamber in order to achieve accurate chamber pressure readings.

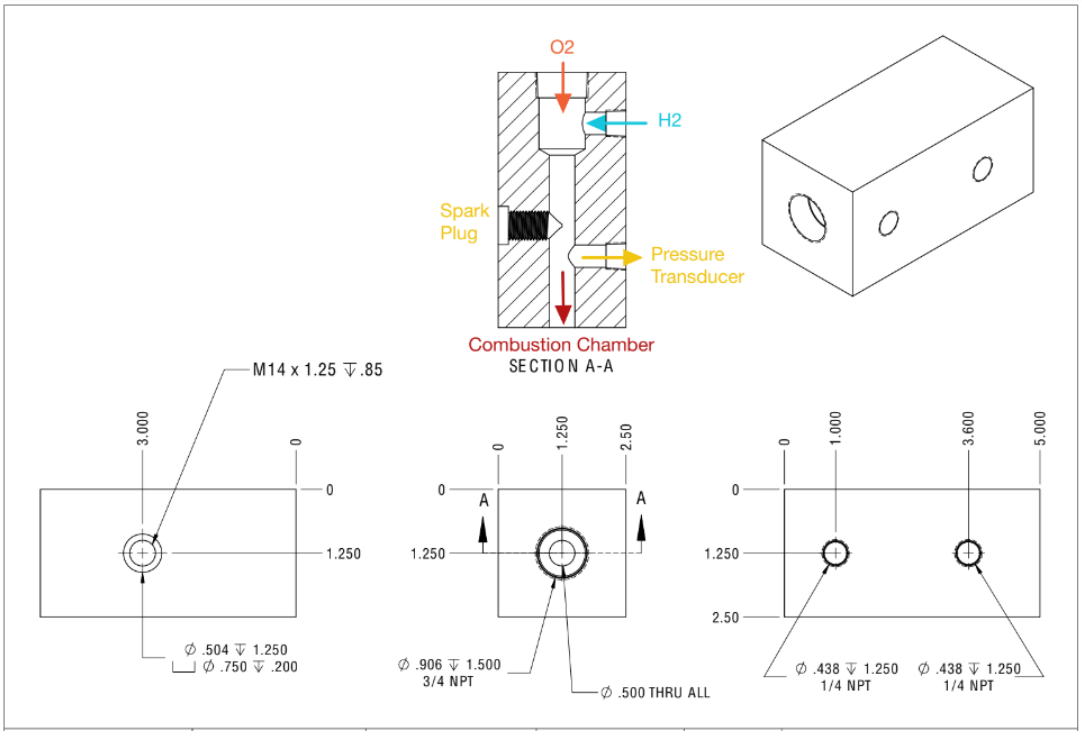

Figure 4.1. Injector block manifold [58].

The combustion chamber cylinder was constructed out of AISI 304 stainless steel pipe and was utilized to provide a secure housing for the nylon 6 fuel grains. As shown in Figure 4.2, the cylinder is 10.16 cm (4 in) in diameter and 30.48 cm (1 ft) in length. A groove was implemented on both ends of the cylinder to allow the use of a Viton O-ring for sealing purposes at the interfacing points (the injector block and the post-chamber structural block).

Figure 4.2 Combustion chamber cylinder [58].

To identify if the combustion chamber cylinder was optimized for the desired chamber pressure during firing, a stress analysis was conducted. A longitudinal stress value was derived from Equation 4.1:

$$\sigma_{longitudinal} = \frac{p_c r_c}{2t} \tag{4.1}$$

where r_c is the radius of the chamber cylinder [m] and t is the cross-sectional thickness of the chamber cylinder [m]. A hoop stress was subsequently found by simply doubling the longitudinal stress. Lastly, an aggregated stress was found from Equation 4.2:

$$\sigma_{total} = \sqrt{\sigma^2{}_{hoop} - \sigma_{hoop}\sigma_{longitudinal} + \sigma^2{}_{longitudinal}} \tag{4.2}$$

where σ_{total} is the total stress that the chamber cylinder is experiencing [Pa]. A Von Mises stress criterion was utilized to ensure satisfactory resilience of the cylinder at the operating chamber pressure of 1.034 MPa (150 psi). This was completed by comparing the total stress of the chamber to AISI 304's tensile yield strength of 215 MPa. This resulted in a safety factor of 38.9. This was above any value that would raises concern for possible redesign. Yet, for a more detailed evaluation, a static structural finite element analysis was also conducted on the combustion chamber cylinder to identify any design vulnerabilities.

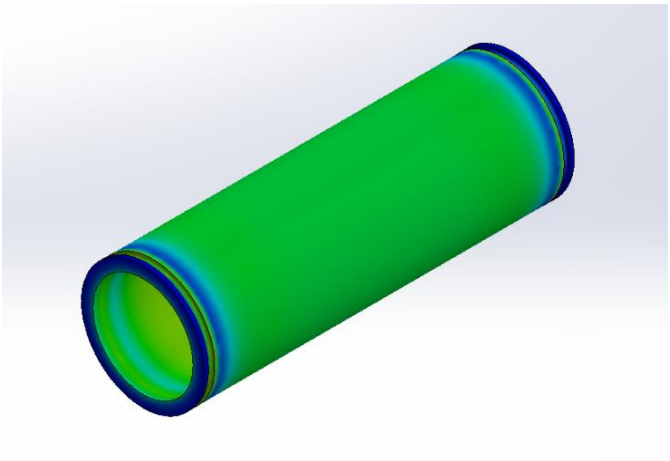

Figure 4.3. Stress mapping from FEA.

Miniscule stress concentrations were found near the O-ring grooves. A maximum stress was found in this area of 8,184,579 Pa. Yet, when compared to the tensile yield strength of AISI 304, a safety factor of 26.3 was calculated and further validated that the chamber structure would be able to withstand the targeted experimental pressures it was designed for.

Lastly, a post-chamber structural block (machined from AISI 304 stainless steel) was implemented to supply a secure mount for a converging-diverging nozzle as well as a back plate to fasten the combustion chamber cylinder. Four 16-inch threaded dowel rods were inserted through the post-chamber structural block and threaded through the injector block in order to press fit the combustion chamber cylinder. Washers and nuts were applied to the threaded dowel rods and installed to approximately 20.3373 N-m (15 ft-lbs) of torque.

The rocket propulsion system was fixated onto a rectangular test stand composed of flat and angled perforated sheet metal strips. A guide rail was installed onto the top of the structure to allow the propulsion system to move linearly during a firing. The injector block and post-chamber structural block were attached onto carriages that would (upon oiling) move freely along the linear guide rail. Two 8-inch threaded dowel rods were fastened vertically through both steel blocks, securing them to the carriages via a rigid plastic platform, as seen in Figure 4.4.

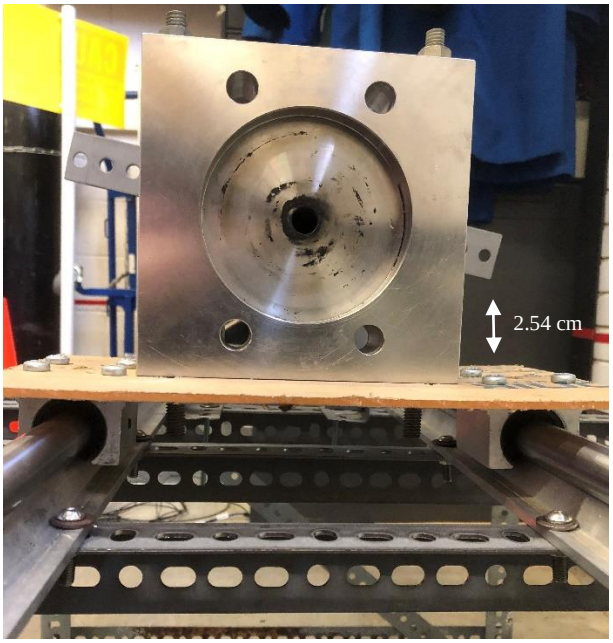

Figure 4.4. Static fire fixture and guide rail interface [58].

A truss structure also composed of perforated sheet metal was secured in front of the injector block, near the end of the guide rails. This structure would provide a secure mount for a force transducer that would be utilized to capture thrust force readings. A final shield composed from stainless steel sheet metal was fabricated and secured over the guide rails and static fire fixture to add a layer of protection from any possible propellant leaks or debris. This test stand was designed to be mobile and can be situated in any ideal location for static fire experiments such as fume hood. A full view of the test stand structure with the static fire fixture can be seen in Figure 4.5 below.

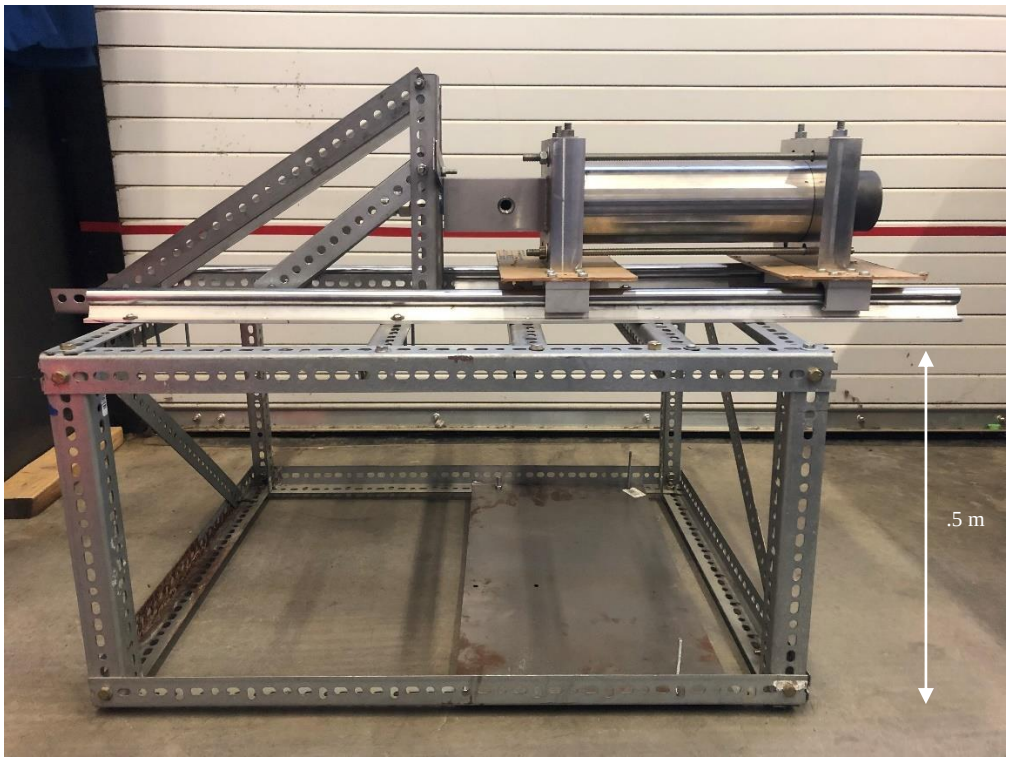

Figure 4.5. Isolated test stand.

4.1.2 Piping System

A detailed piping system was constructed utilizing both electrical and manual components for fluid flow control. With experimental run procedures in mind, a dedicated fluid line was created for each propellant in the system: oxygen, hydrogen, and nitrogen (for purging purposes). A detailed piping and instrument diagram (P&ID) created for experimental procedures is shown below in Figure 4.6.

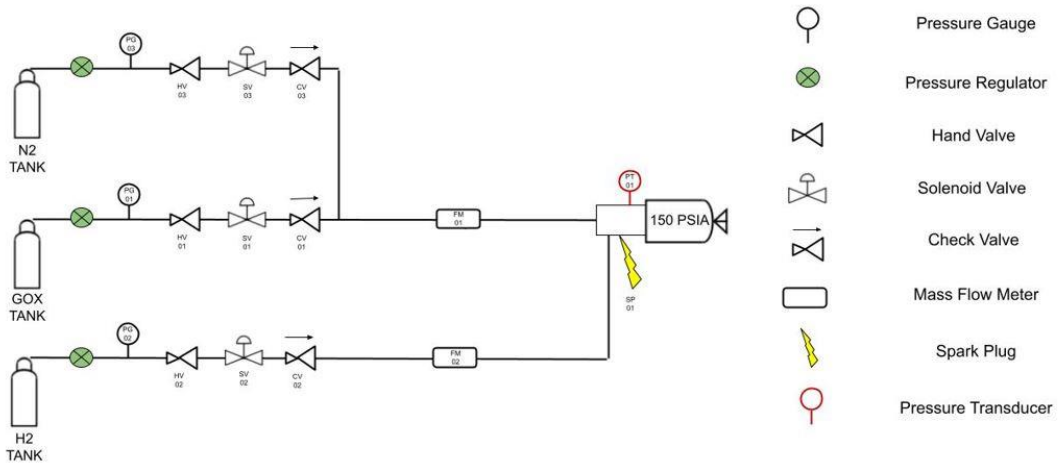

Figure 4.6. Simplified P&ID of propellant fluid systems.

Each propellant was contained in a K-type cylinder with an attached pressure gauge and regulator. Each propellant line contained a manual hand valve, a solenoid valve, and a check valve. The hand valves were implemented to manually control the flow of propellant from the gas tanks. The solenoid valves were utilized to have an automatic method of opening and closing the propellant lines during run procedures. Lastly, the check valves were included to prevent any backflow into other fluid system components which could cause damage. The nitrogen line was constructed to merge into the oxygen line after each of their check valves. This was done because of the single oxidizer inlet at the injector block. An Aalborg GFM77 mass flow meter was attached in both of the inlet propellant lines to measure the rate of mass flow for experimental procedures. However, these meters were calibrated for air. Therefore, under the manufacturer's guidelines, an empirically found calibration factor (or 'k-factor') was multiplied to each propellant's flow rate readings to get an accurate result. In respect to air, oxygen's k-factor is .9926 and hydrogen's k-factor is 1.9 (see Appendix A). Due to no mass flow controllers for the desired experimental mass flow rates being available at the laboratory, the mass flow rates were found empirically by altering the pressure regulator until the targeted rates were

acquired on the meters. The oxygen and nitrogen propellant lines were .9525 cm (.375 in) in diameter, and the hydrogen line was .635 cm (.25 in) in diameter. These sizes were chosen based on fluid simulations ran on each propellant that compared pressure drop to line length on various diameter sizes.

4.1.3 Nozzle Design

The nozzle for the hybrid rocket propulsion system was designed utilizing values derived from the theoretical approach. This included a throat diameter of 7.62 mm (.3 in), an expansion ratio of 1.95, and an exit diameter of 10.64 mm (.419 in). A conical (as opposed to a bell) configuration was decided for ease of manufacturing purposes. The half angle for the diverging portion of the design was chosen to be 12 degrees, as seen in Figure 4.7. Typical half angle values for conical nozzles range from 12 to 18 degrees, depending on the desired length of the diverging portion. Yet, smaller diverging half angles yield higher nozzle efficiencies, as seen in Equation 4.3 [8]:

$$\lambda = \frac{1}{2}(1 + cos\theta_{cn}) \tag{4.3}$$

where λ is the nozzle efficiency and θ_{cn} is the nozzle cone half angle [°]. This is due to the reduction of thrust loss from the decreased radial-velocity component. Therefore, a 12-degree half angle (24-degree total angle) was chosen to achieve the highest efficiency for a reasonable diverging section length of 7.112 mm (.28 in). This resulted in a converging portion length of 69.088 mm (2.720 in) to achieve an overall nozzle length of 76.2 mm (3 in), also seen in Figure 4.7.

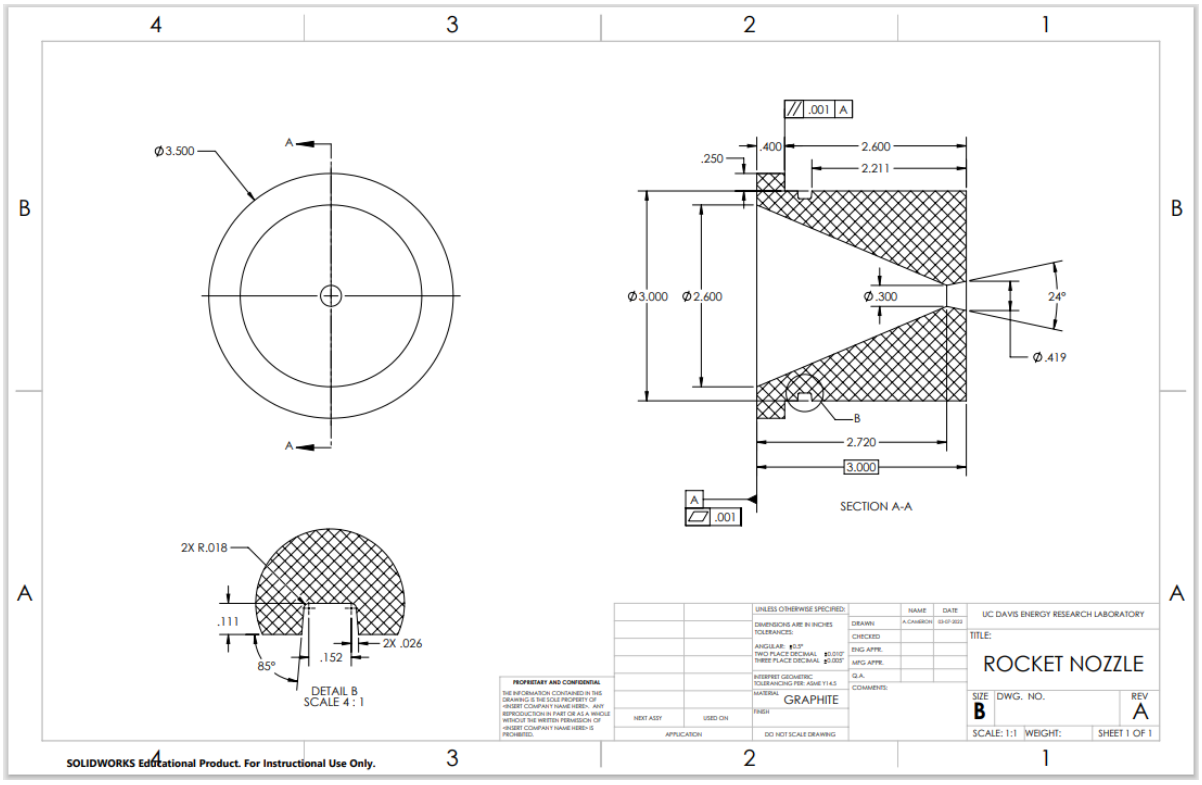

Figure 4.7. Rocket nozzle drawing.

The nozzle was machined out of graphite — a typical selection for rocket nozzles for its thermal properties such as high temperature resistance [75]. This component fits through the post-chamber structural block and is securely press fitted once the combustion chamber cylinder is inserted. A Viton O-ring was attached to the nozzle in the groove before insertion for sealing purposes.

4.1.4 Fuel Grain Preparation

Nylon 6 fuel grains were acquired from Mitsubishi Chemical Advanced Materials. The solid thermoplastic cylinders arrived 12 inches in length; however, due to wide stock tolerances from the manufacturer, fabrication needed to be completed on the outer diameter. This was to ensure a secure press fit into a cardboard sleeve before placing it inside the combustion chamber for sealing purposes and inner cylinder protection. A lathe was utilized to discard .635 centimeters

(.25 inches) of the grain so a perfect 7.62 cm (3 in) outer diameter could be achieved. Lastly, a central port hole was machined utilizing a cordless drill. After a pilot hole was drilled, a 1.27 cm (.5 in) bit was utilized on both ends of the fuel grain to obtain the initial bore size. The final geometry of the fuel grains can be seen below in Figure 4.8.

Figure 4.8. Top view of nylon 6 fuel grain inserted into sleeve.

4.1.5 Electrical Systems

An Ardunio Uno was identified as an appropriate microcontroller to command and manage the electrical components of the propulsion system. With a nearby breadboard, all data-reading components such as the force and pressure transducer could be connected, and data logging could occur using a supplemental program such as PuTTY. The propellant mass flow rates could also be logged from their respective meters and would allow the experimenter to monitor levels during system operation. The solenoid valves were also controlled by the Ardunio through the means of three electrical relays that would provide them with the appropriate voltage signal. Depending on the run procedure of any given experiment for the hydrogen co-firing studies, the flow from the propellant tanks (oxygen, hydrogen, and nitrogen) could be controlled to any time

sequence needed. The solenoids could also be controlled to be turned on after such sequence for any additional purposes (such as nitrogen purging).

The spark plug circuit implemented in the propulsion system's injector block consisted of a Bosch spark plug, a condenser, ignition coil, a 12-volt battery, and a manual toggle switch (as seen in Figure 4.9). With the manual toggle switch, the experimenter could manually control when to begin the combustion process. When flipped into the "on" position, the circuit is completed, and the 12 V signal from the battery is transformed by the ignition coil into the proper voltage needed for the spark plug to create the spark.

Figure 4.9. Isolated spark plug assembly components.

Chapter 5

Simulation Approach

In order to assess the performance of the hybrid rocket propulsion system design, as well as draw conclusions on how the addition of hydrogen supplements the overall combustion event of the rocket, simulations were run using NASA CEA software at the desired operational levels. The two main combustion events that were analyzed included the baseline burn of the gaseous oxygen and nylon 6 thermoplastic fuel grain as well as the upstream burn of gaseous hydrogen and gaseous oxygen. The baseline burn, over the GH_2/GO_x burn, was assessed for performance parameters as its fuel and oxidizer combination could be analyzed as a stand-alone hybrid rocket propulsion system under the assumption of a non-hydrogen induced ignition source, such as a pyrotechnic igniter. It is important note that this burn, unlike the GH_2/GO_x combination, requires an extra endothermic pyrolysis step to begin liberating the fuel molecules from a solid, thermoplastic state to a gaseous state. The GH_2/GO_x burn, on the contrary, solely requires activation energy (ideally from a spark plug) to begin combustion, as they are in the same physical state. The GH_2/GO_x combustion event was analyzed to understand the role that its upstream flame might have as it propagates down the nylon 6 fuel grain port. In order for NASA CEA software to compute accurate results, a few inputs are first required. The operating

combustion chamber pressure, nozzle pressure ratio, propellant configuration, and desired O/F ratios are all variables that are required for calculations to ensue. Additionally, a specification must be made to whether the program utilizes an equilibrium or frozen flow assumption. Under an equilibrium assumption, the chemical reactions within the combustion chamber occur very quickly and the gas composition is allowed to change throughout the nozzle. Under a frozen flow assumption, the chemical reactions are assumed to occur very slowly and that the composition of the combustion gases within the chamber do not change on its path through and out of the nozzle. For the purposes of the combustion analyses, equilibrium flow was assumed in order to identify a more accurate breakdown of species within the exhaust gases. A wide array of O/F ratios were examined for each combustion simulation, with priority attention given to the targeted O/F ratio of 16.

5.1 Gaseous Oxygen and Nylon 6 Combustion

The baseline simulation analysis was conducted on the gaseous oxygen and nylon 6 burn. This burn reflects traditional hybrid rocket propulsion systems where a single fuel and oxidizer are included in the combustion process. On a mass basis, a gaseous oxygen and nylon 6 propellant combination hosts a stochiometric O/F ratio of 2.33, assuming complete combustion — important to note when evaluating the simulation results. Before performing the simulation, the aforementioned operating inputs, as well as a mass-basis chemical breakdown of nylon 6, were included in the set up. The first performance parameter that was analyzed was the system's characteristic exhaust velocity over a spectrum of O/F ratios, as shown in Figure 5.1.

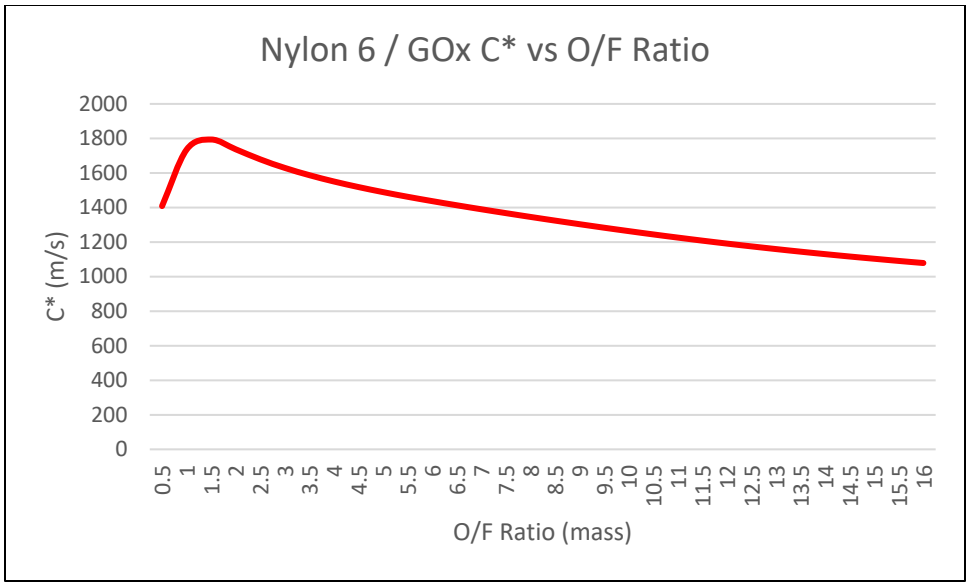

Figure 5.1. Nylon 6 and GOx C* as a function of O/F ratio.

It can be seen that the general trend of the characteristic exhaust velocity with the gaseous oxygen and nylon 6 burn is a notable increase around fuel-rich conditions, and after stochiometric ratios a light descent toward higher fuel-lean conditions. Assuming experimental-like results from the CEA simulation, a comparison to the theoretical design was made in order to find overall propellant performance. This was executed by utilizing Equation 5.1 [35]:

$$\eta_c = \frac{C^*_{simulated}}{C^*_{theoretical}} \tag{5.1}$$

where η_c is the combustion efficiency of the propulsion system. The characteristic exhaust velocity was taken from the simulation at the desired fuel-lean operating level of a 16 O/F ratio. At 1078.8 m/s, the system's propellant performance proved to be rather strong with an overall combustion efficiency of 83.67%. Experimental findings will further validate the combustion efficiency of the propulsion system.

The next performance parameter that was evaluated from the gaseous oxygen and nylon 6 burn was the specific impulse. The results from the CEA simulation would elucidate how well

the propulsion system converts its mass flow rates into useful thrust. The graph of the baseline's specific impulse performance can be seen below in Figure 5.2.

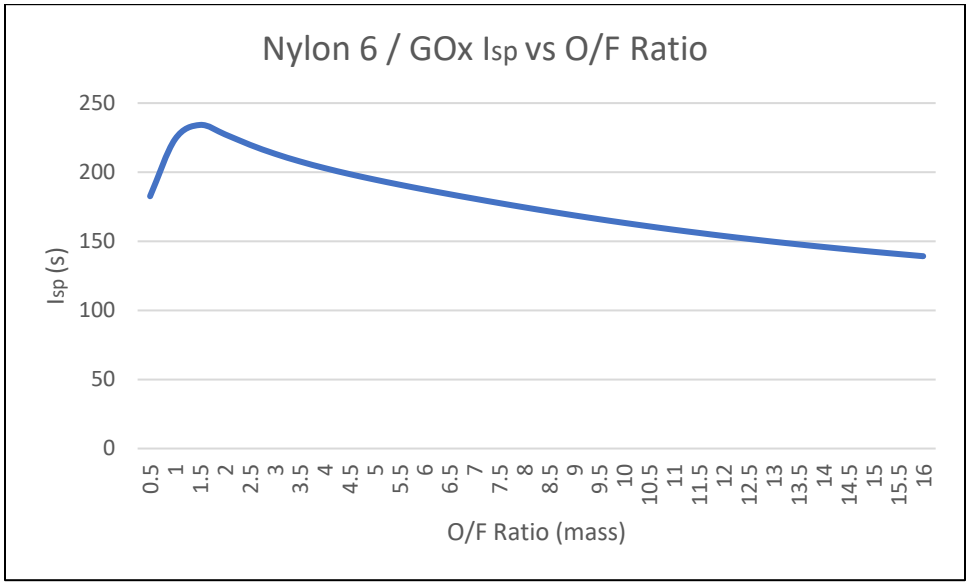

Figure 5.2. Nylon 6 and GOx Isp as a function of O/F ratio.

Similar to the characteristic exhaust velocity, it appears peak performance of the propulsion system occurs in the slightly fuel-rich region. A gentle decline occurs as the O/F ratios continue to rise, and at the desired 16 O/F ratio a specific impulse of 139.2 seconds is attained. With this piece of information acquired, the overall engine performance can be evaluated by utilizing Equation 5.2:

$$\eta_{system} = \frac{Isp_{simulated}}{Isp_{theoretical}} \tag{5.2}$$

where η_{system} is the efficiency of the entire propulsion system. This relationship yielded an overall system efficiency of 83.95 %. Experimental results will further validate this efficiency as well.

5.2 Gaseous Oxygen and Gaseous Hydrogen Combustion

The gaseous oxygen and gaseous hydrogen burn begins within the injector block, and once a flame is established, propagates downstream into the fuel grain port. Therefore, it is of critical importance that characteristics of the GH_2/GO_x burn are explored so conclusions can be made on its impact toward the overall rocket combustion event. Under the assumption of complete combustion, the stochiometric O/F ratio for oxygen and hydrogen is 8 on a mass basis. The first attribute from the propellant combination that was explored was the characteristic exhaust velocity, as seen in Figure 5.3.

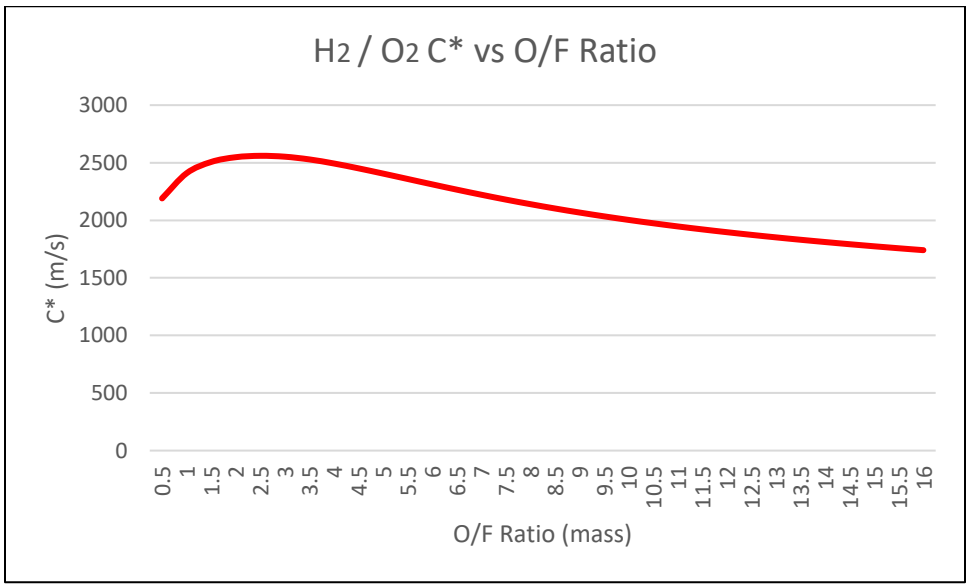

Figure 5.3. H_2 and O_2 C* as a function of O/F ratio.

It can be seen from the graph that the GH_2/GO_x burn produces significantly higher characteristic exhaust velocities than the nylon $6/GO_x$ burn over all evaluated O/F ratios. Due to the unique combustive properties that hydrogen possesses, including energetic content, it is understandable that at similar fixed variables (throat area and mass flow rate) a higher chamber pressure (and thus C*) could be achieved. At the desired 16 O/F ratio, the GH_2/GO_x burn

produces a characteristic exhaust velocity of 1740.5 m/s — 61.33% larger than that of the nylon 6 burn. It can be seen from Figure 5.4 below that the GH_2/GO_x burn also produces significantly higher specific impulses than the nylon $6/GO_x$ combustion event over all evaluated O/F ratios.

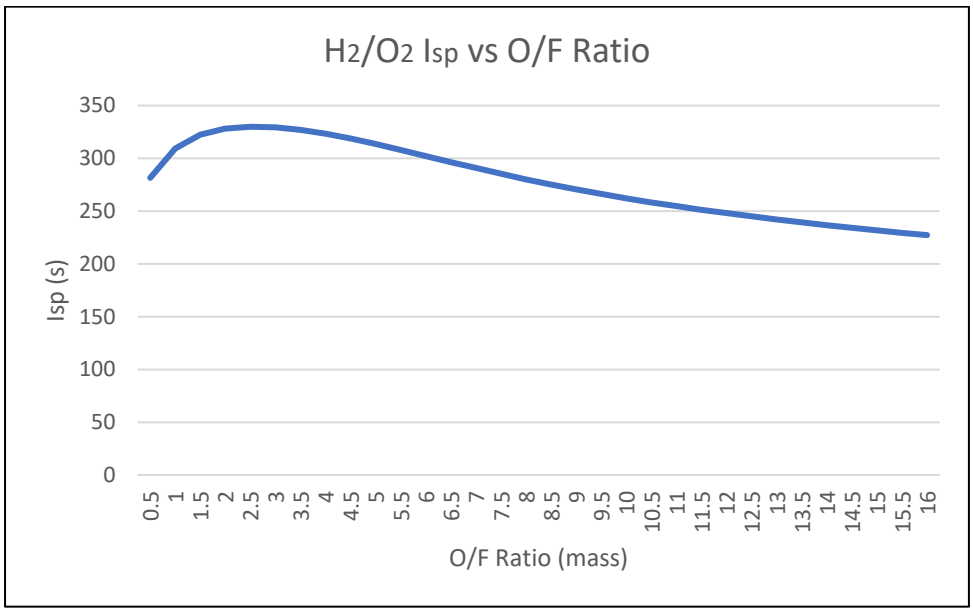

Figure 5.4. H_2 and O_2 Isp as a function of O/F ratio.

Another key characteristic that was examined was the combustion temperature produced from the GH_2/GO_x propellant combination. NASA CEA produces three different results for flame temperatures based on the area of interest: the chamber, the nozzle throat, and the nozzle exit. Considering the nozzle throat and nozzle exit are downstream of the nylon 6 fuel grain itself, only chamber combustion temperature was analyzed. As seen in Figure 5.5, the GH_2/GO_x burn produces rather low combustion temperatures in the fuel-rich region. It is not until stochiometric conditions are met that a peak temperature is achieved (3393.38 K at 8 O/F). However, the advantageous trait that this burn presents is a relatively steady combustion temperature in the fuel-lean region. The temperature stays quite high at O/F ratios from 4-16, with no steep drop offs in that range. It is inferred that at the elevated combustion temperatures

the heat transfer from the GH_2/GO_x flame to the solid nylon 6 fuel grain wall would increase in comparison to a non-hydrogen produced flame, thus promoting the pyrolysis event.

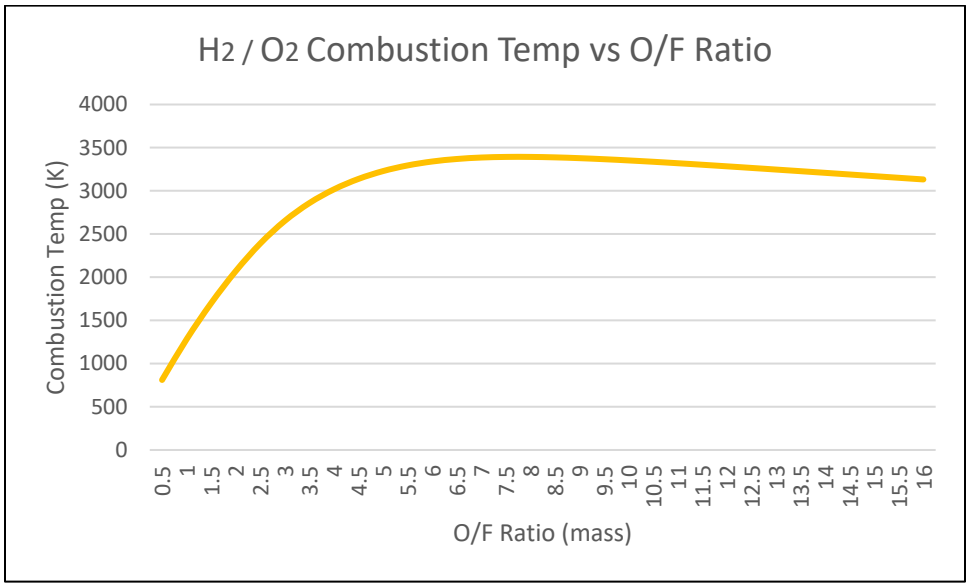

Figure 5.5. H_2 and O_2 combustion temperature as a function of O/F ratio.

It is apparent that the thermodynamic properties of the GH_2/GO_x burn have the potential to increase the heat transfer to the nylon 6 fuel grain, and, furthermore, increase the amount of pyrolyzed thermoplastic into the total propellant stream. Yet, other key factors that are vital to decoding the overall combustion mechanisms of the propulsion system include the emissions from the GH_2/GO_x burn. Due to the co-firing configuration, the oxidizer is in contact with two different fuel sources in its axial path toward the nozzle. Therefore, an investigation into the availability of prominent oxidizing molecules was performed. Unbounded oxygen atoms were first assessed over the O/F ratio range, as shown in Figure 5.6 below.

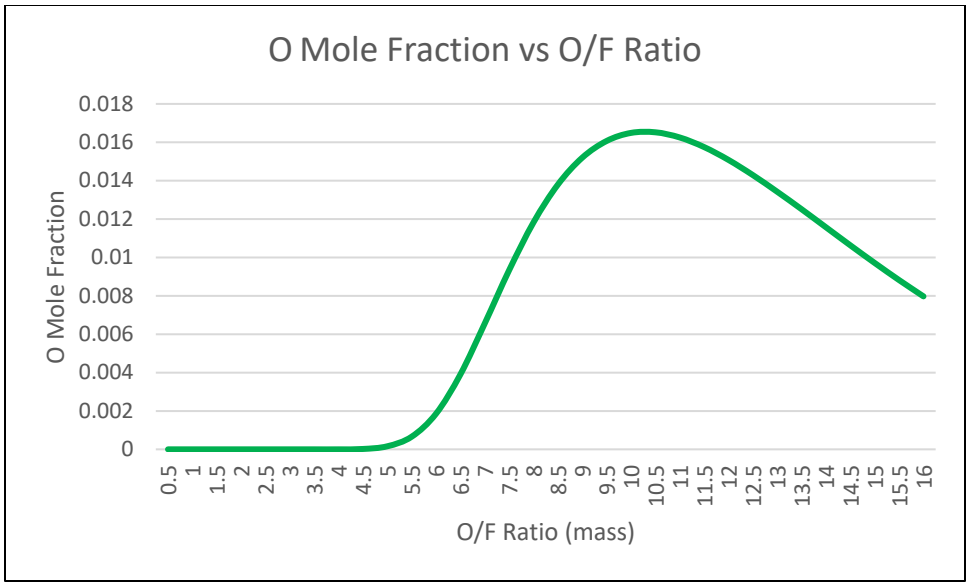

Figure 5.6. O mole fraction as a function of O/F ratio (mass) for H_2 and O_2 burn.

It is apparent that in the fuel-rich region of the GH_2/GO_x burn there is little to no oxygen atoms available for the pyrolyzed volatile hydrocarbons released from the nylon 6 to combust with. It is not until slightly fuel-lean ratios are achieved that a surplus of the atoms are released. Normal oxygen molecules were also examined, as seen in Figure 5.7.

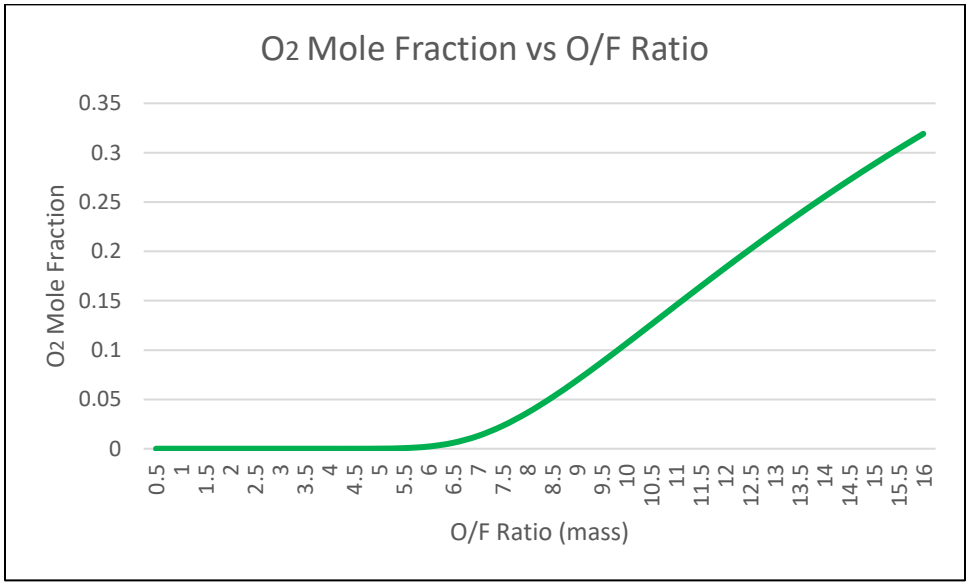

Figure 5.7. O_2 mole fraction as a function of O/F ratio (mass) for H_2 and O_2 burn.

In a similar fashion, the fuel-rich region of the GH_2/GO_x burn yields no available oxygen molecules. However, an approximate linear relationship is present from stochiometric conditions up until an O/F ratio of 16. In fact, the peak of the oxygen molecules is present at the desired operating level of a 16 O/F ratio. Lastly, hydroxide compounds were examined, as shown in Figure 5.8.

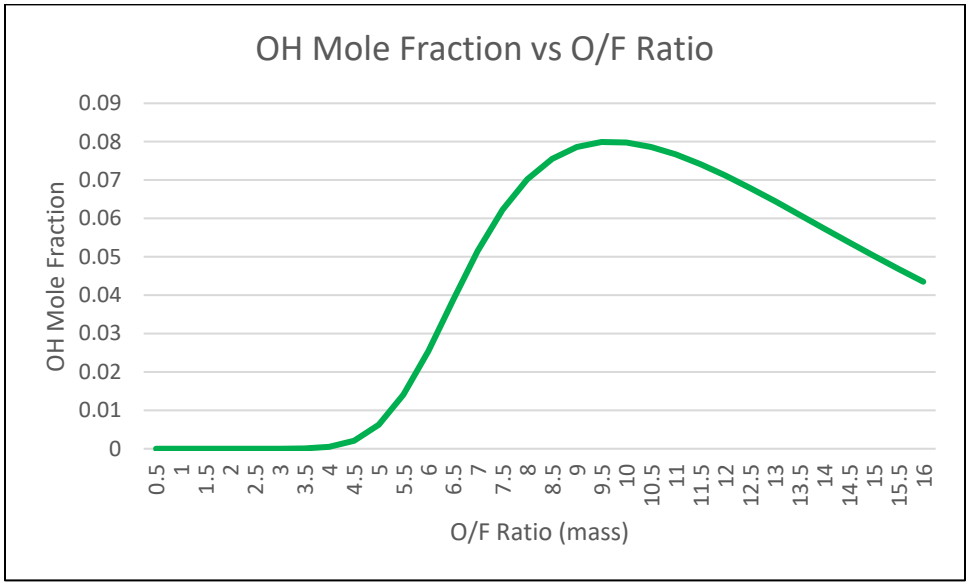

Figure 5.8. OH mole fraction as a function of O/F ratio (mass) for H_2 and O_2 burn.

The hydroxide mole fraction followed a similar pattern as the unbounded oxygen atoms. In the fuel-rich O/F ratios, there are no compounds present. Yet, once slightly fuel-lean conditions are reached, a peak amount can be found.

It is evident that at fuel-lean conditions of the GH_2/GO_x burn an excess of oxidizing molecules are present. Although the mole fractions of the oxygen atoms and hydroxide compounds are rather small, the amount of diatomic oxygen molecules that are found at the desired O/F ratio of 16 are significant. This leads to the postulation that the pyrolyzed nylon 6 fuel grain would have appropriate access to oxidizing molecules during the firing of the propulsion system. In addition to higher temperatures brought from the GH_2/GO_x flame, it is

posited that the hydrogen co-firing configuration could provide increased regression rates of the nylon 6 fuel grain and enhanced performance parameters for the hybrid rocket propulsion system.

Chapter 6

Conclusions

6.1 Concluding Remarks

With hybrid rockets continuing to grow as useful technologies for delivering small payloads into low earth orbit, it is critical strategies focused on increasing fuel consumption rates (and thus combustion efficiencies) are created to ensure effective mission operation. In this study, a hybrid rocket propulsion system was designed and manufactured for the purposes of exploring hydrogen co-firing as a valid regression and performance-enhancing technique that the accompanying limited literature seems to convey. Theoretical maximum performance parameters of the propulsion system were found for the purposes of comparison to simulation results as well as future experimental data. It was established through the utilization of NASA CEA software that the baseline propellant combination of nylon 6 and gaseous oxygen is likely to operate with an 83.67% combustion efficiency and an 83.95% overall system efficiency, given a non-hydrogen ignition source. It was shown that the separate upstream burning of the gaseous hydrogen and gaseous oxygen could produce significantly high combustion temperatures and pressures. It is posited that as the flame propagates down the nylon 6 fuel grain, it would enhance the heat

transfer to the thermoplastic surface and expedite the pyrolysis event — especially at lean O/F ratios. Yet, equally interesting is the rise in available oxidizing molecules that the pyrolyzed nylon 6 hydrocarbons could combust with once stochiometric to fuel-lean operations are met. Conversely, at fuel-rich O/F ratios, there would be little to no oxidizer for the pyrolyzed thermoplastic. This could cause significant system failures such as misfires, especially if the hydrogen is simply used as a fuel burst instead of being continuously propelled into the chamber. Therefore, it is postulated that the hydrogen co-firing configuration would not be ideal to run at fuel-rich O/F ratios, and that at very fuel lean proportions (16 or higher) the thermoplastic fuel grain would get the most available oxidizing molecules. This supports the current experimental data found within literature. Ultimately, it appears that the use of the hydrogen co-firing configuration would promote the heat and mass transfer mechanisms that notoriously limit hybrid rocket propulsion systems. Due to time constraints and the importance of preliminary analysis before firing, experiments utilizing the propulsion system were not performed within the scope of this paper.

6.2 Recommendations for Future Works

With a physical hybrid rocket propulsion system built, and detailed simulation analysis performed, the next logical step would be to evaluate the experimental performance of the engine at the targeted O/F ratio of 16. One unique study could utilize hydrogen addition time as an independent variable to see how much hydrogen would be needed to increase regression rates and performance parameters. Due to existing literature showcasing hydrogen's abilities at stochiometric to fuel-lean O/F ratios, this study could elaborate on what quantity of the gas would be needed to deliver a small satellite (or CubeSat) payload into low earth orbit. Subsequently, utilizing the pressure and force transducer implemented in the system, combustion

and system efficiencies can be found by comparing the experimental results to that of the theoretical design. This could further be compared to the CEA results, and conclusions can be drawn on the differences between a theoretical, simulation, and experimental approach. Not only would this validate the limited existing literature on hydrogen's performance-enhancing properties, but further authenticate the utilization of the hydrogen-oxygen torch igniter as a premier ignition source for hybrid rocket propulsion systems.

Another prominent study that could be tackled would be an investigation into the emissions of the propulsion system with the hydrogen co-firing configuration. There is very little existing literature pertaining to rocket emissions, let alone hybrid systems. Therefore, it would be unique not only to map the combustion products of the baseline propellant combination of gaseous oxygen and nylon 6, but to investigate if any competition for oxidizing molecules arises with the use of supplemental hydrogen. Exhaust species could be examined over a plethora of O/F ratios to see whether hydrogen co-firing could minimize certain adverse pollutants or greenhouse gases. This would be vital information, as the number of hybrid rocket firings — amongst all types of chemical propulsion systems — are continuing to grow.

Other future works that could be very insightful to the hybrid rocket propulsion discussion could be altering both the fuel grain and supplemental propellant selection for the co-firing configuration. There are plenty of other thermoplastic polymers that have proven to show advantageous regression rates, such as ASA. A performance comparison between classical choices such as ABS and novel polymer formulations could be beneficial to identifying ideal propellant combinations. Likewise, combustion products of various thermoplastics could also be explored to recognize clean fuel selections. The supplemental fuel source could be swapped out for other candidates, such as methane. This would not only further authenticate the use of a

methane-oxygen torch igniter but allow exploration of regression rates and performances to be completed as well. Additionally, the supplemental propellants could be pulse fired into the combustion chamber — a strategy to characterize the cold start capabilities that hybrid rockets are renowned known for.

References

[1] "Commercial Space Data." *Federal Aviation Administration*, 4 Jan. 2022, https://www.faa.gov/data_research/commercial_space_data/.

[2] "CubeSats." *The European Space Agency*, 31 Mar. 2022, https://www.esa.int/Enabling_Support/Preparing_for_the_Future/Discovery_and_Preparation/CubeSats.

[3] Mabrouk, Elizabeth. "What Are SmallSats and CubeSats?" *NASA*, NASA, 13 Mar. 2015, https://www.nasa.gov/content/what-are-smallsats-and-cubesats.

[4] "CubeSats and SmallSats." Edited by Tony Greicius and Naomi Hartono, *Jet Propulsion Laboratory*, NASA, https://www.jpl.nasa.gov/topics/cubesats.

[5] "Nanosatellite and Microsatellite Market Size Report 2030." *Grand View Research*, Grand View Research, Inc, https://www.grandviewresearch.com/industry-analysis/nanosatellite-microsatellite-market.

[6] "Small Satellite Market Size, Growth & Global Forecast [2028]." *Fortune Business Insights*, https://www.fortunebusinessinsights.com/industry-reports/small-satellite-market-101917.

[7] "Virginia CubeSat Constellation." *Virginia CubeSat Constellation*, https://vsgc.odu.edu/virginiacubesatconstellation/.

[8] Humble, Ronald W., et al. *Space Propulsion Analysis and Design*. McGraw-Hill, 2007.

[9] Schmierer, Christian, et al. "Low Cost Small-Satellite Access to Space Using Hybrid Rocket Propulsion." *Acta Astronautica*, Elsevier Ltd, 16 Feb. 2019.

[10] "Vaya Space." *Vaya Space*, https://www.vayaspace.com/.

[11] "Access to space with hybrid propulsion." *HyImpulse*, https://www.hyimpulse.de/en/.

[12] “BluShift Aerospace.” *BluShift Aerospace,* https://www.blushiftaerospace.com/.

[13] Knuth, William H. et al. “Solid-Fuel Regression Rate Behavior of Vortex Hybrid Rocket Engines.” *Journal of Propulsion and Power*, vol. 18, no. 3, May 2002.

[14] Messineo, Jérôme, and Toru Shimada. “Theoretical Investigation on Feedback Control of Hybrid Rocket Engines.” *Aerospace,* vol. 6, no. 6, June 2019, p. 65.

[15] Sutton, George P., and Oscar Biblarz. *Rocket Propulsion Elements*. 8th ed., Wiley, 2017.

[16] “Rocket Engines Designed for Reuse.” *Blue Origin*, https://www.blueorigin.com/engines/.

[17] “Falcon 9.” *SpaceX*, https://www.spacex.com/vehicles/falcon-9/.

[18] Herakovich, Carl T. *Mechanics of Fibrous Composites*. John Wiley and Sons, Inc., 1998.

[19] McFarland, Mitchell, and Elsa Antunes. "Small-Scale Static Fire Tests of 3D Printing Hybrid Rocket Fuel Grains Produced from Different Materials" *Aerospace,* vol. 6, no. 7, July 2019, p. 81.

[20] Grefen, Benedict, et al. “Design, Production and Evaluation of 3D-Printed Mold Geometries for a Hybrid Rocket Engine.” *Aerospace*, vol. 8, no. 8, Aug. 2021, p. 220.

[21] “Virgin Galactic.” *Virgin Galactic,* https://www.virgingalactic.com/.

[22] Kopacz, Wioleta, et al. “Hydrogen Peroxide – a Promising Oxidizer for Rocket Propulsion and Its Application in Solid Rocket Propellants.” *FirePhysChem*, vol. 2, no. 1, Mar. 2022, pp. 56–66.

[23] Whitmore, Stephen A. “Nytrox as ‘Drop-in’ Replacement for Gaseous Oxygen in SmallSat Hybrid Propulsion Systems.” *Aerospace,* vol. 7, no. 4, Apr. 2020, p. 43.

[24] Glassman, Irvin et al. *Combustion.* 5th ed., Elsevier, 2015.

[25] Marquardt, Timothy, and Joseph Majdalani. “Review of Classical Diffusion-Limited Regression Rate Models in Hybrid Rockets.” *Aerospace*, vol. 6, no. 6, June 2019, p. 75.

[26] Karabeyoglu, M. Arif and Greg Zilliac. “Hybrid Rocket Fuel Regression Rate Data and Modeling.” *Joint Propulsion Conferences*, 18 June 2012.

[27] Marxman, G. A. et al. “Fundamentals of Hybrid Boundary Layer Combustion.” *Heterogenous Combustion*, 1964, pp. 485-522.

[28] Judson, Michael I. Jr. *Direct Electrical Arc Ignition of Hybrid Rocket Motors*. 2015. Utah State University, Master’s Thesis. https://digitalcommons.usu.edu/etd/4149/.

[29] Castaneda, David A., and Benveniste Natan. “Experimental Investigation of the Hydrogen Peroxide – Solid Hydrocarbon Hypergolic Ignition.” *Acta Astronautica*, vol. 158, May 2019, pp. 286–295.

[30] Repas, George A. “Hydrogen-Oxygen Torch Ignitor.” *National Aeronautics and Space Administration*, Mar. 1994.

[31] Shynkarenko, Olexiy, and Domenico Simone. “Oxygen–Methane Torch Ignition System for Aerospace Applications.” *Aerospace*, vol. 7, no. 8, Aug. 2020, p. 114.

[32] Conte, Antonietta, et al. “Design, Modeling and Testing of a O2/CH4 Igniter for a Hybrid Rocket Motor.” *2018 Fluid Dynamics Conference*, June 2018.

[33] Chen, Suhang, et al. “Innovative Methods to Enhance the Combustion Properties of Solid Fuels for Hybrid Rocket Propulsion.” *Aerospace*, vol. 6, no. 4, Apr. 2019, p. 47.

[34] Battista, Francesco, et al. “Design and Testing of a Paraffin-Based 1000 N HRE Breadboard.” *Aerospace*, vol. 6, no. 8, Aug. 2019, p. 89.

[35] Heeg, Francesca et al. “Design and Test of a Student Hybrid Rocket Engine with an External Carbon Fiber Composite Structure.” *Aerospace*, vol. 7, no. 5, May 2020, p. 57.

[36] Pastrone, David. “Approaches to Low Fuel Regression Rate in Hybrid Rocket Engines.” *International Journal of Aerospace Engineering*, vol. 2012, Article ID 649753, 12 pages, 2012. https://doi.org/10.1155/2012/649753.

[37] Whitmore, Stephen A., et al. “High Regression Rate Hybrid Rocket Fuel Grains with Helical Port Structures.” *Journal of Propulsion and Power*, vol. 31, no. 6, Nov. 2015, pp. 1727–1738.

[38] Kim, Soojong, et al. “Regression Characteristics of the Cylindrical Multiport Grain in Hybrid Rockets.” *Journal of Propulsion and Power*, vol. 29, no.3, 7 May 2013.

[39] Ahn, Byeonguk et al. “Design of Multiport Grain with Hydrogen Peroxide Hybrid Rocket.” *Journal of Propulsion and Power*, vol. 34, no. 5, Sep. 2018.

[40] Whitmore, Stephen A. “Three-Dimensional Printing of ‘Green’ Fuels for Low-Cost Small Spacecraft Propulsion Systems.” *Journal of Spacecraft and Rockets*, vol. 55, no. 1, Jan. 2018, pp. 13–26.

[41] Young, Gregory et al. “Examining Port Geometry/Solid Loading for Additively Manufactured Fuels in Hybrid Rockets.” *Journal of Propulsion and Power*, vol. 37, no. 2, Mar. 2021.

[42] Piscitelli, F., et al. “Characterization and Manufacturing of a Paraffin Wax as Fuel for Hybrid Rockets.” *Propulsion and Power Research*, Elsevier, 31 Aug. 2018.

[43] Di Martino, Giuseppe Daniele, et al. “The Application of Computational Thermo-Fluid-Dynamics to the Simulation of Hybrid Rocket Internal Ballistics with Classical or Liquefying Fuels: A Review.” *Aerospace*, vol. 6, no. 5, May 2019, p. 56.

[44] “Sasolwax®.” *SpecialChem*, https://cosmetics.specialchem.com/product/i-sasol-sasolwax-0907.

[45] Bisin, Riccardo, et al. “A New Strategy for the Reinforcement of Paraffin-Based Fuels Based on Cellular Structures: The Armored Grain - Mechanical Characterization.” *Acta Astronautica*, vol.176, Nov. 2020, pp. 494-509.

[46] Veale, Kirsty, et al. “The Structural Properties of Paraffin Wax Based Hybrid Rocket Fuels with Aluminium Particles.” *Acta Astronautica*, Elsevier, 23 July 2018.

[47] Paravan, Christian. “Nano-Sized and Mechanically Activated Composites: Perspectives for Enhanced Mass Burning Rate in Aluminized Solid Fuels for Hybrid Rocket Propulsion.” *Aerospace*, vol. 6, no. 12, Nov. 2019, p. 127.

[48] Sorge, C. Carmicino and A. Russo. “Experimental Investigation into the Effect of Solid-Fuel Additives on Hybrid Rocket Performance.” *Journal of Propulsion and Power*, vol. 31, no. 2, 26 Feb. 2015.

[49] Zhang, Zelin, et al. “Effects of Swirl Injection on the Combustion of a Novel Composite Hybrid Rocket Fuel Grain.” *Acta Astronautica*, vol. 199, Oct. 2022, pp. 174-182.

[50] Knuth, William H., et al. “Solid-Fuel Regression Rate Behavior of Vortex Hybrid Rocket Engines.” *Journal of Propulsion and Power*, vol. 18, no. 3, May 2002, pp. 600–609.

[51] Yuasa, Saburo, et al. “A Technique for Improving the Performance of Hybrid Rocket Engines.” *35th Joint Propulsion Conference and Exhibit*, 1999.

[52] Lee, Changjin, et al. “Effect of Induced Swirl Flow on Regression Rate of Hybrid Rocket Fuel by Helical Grain Configuration.” *Aerospace Science and Technology*, vol. 11, no. 1, 2007, pp. 68–76.

[53] Ohyama, Sho, et al. “A Study of Hybrid Rockets with Multi-Section Swirl Injection Method.” *Joint Propulsion Conferences*, 6 Sept. 2012.

[54] Kornbluth, Kurt et al. “Extension of the lean limit through hydrogen enrichment of a LFG-fueled spark-ignition engine and emissions reduction.” *International Journal of Hydrogen Energy*, vol. 35, no. 3, Elsevier Ltd, 22 Dec. 2009.

[55] Greenwood, J.B. et al. “Experimental results of hydrogen enrichment of ethanol in an ultra-lean internal combustion engine.” *International Journal of Hydrogen Energy*, vol. 39, no. 24, Elsevier Ltd, 5 July 2014.

[56] Amrouche, F., et al. “An Experimental Analysis of Hydrogen Enrichment on Combustion Characteristics of a Gasoline Wankel Engine at Full Load and Lean Burn Regime.” *International Journal of Hydrogen Energy*, vol. 43, no. 41, Elsevier Ltd, 11 Sept. 2018.

[57] Amrouche, F., et al. “An experimental investigation of hydrogen-enriched gasoline in a Wankel rotary engine.” *International Journal of Hydrogen Energy*, vol. 39, no. 16, Elsevier Ltd, 19 Apr. 2014.

[58] Ochi, Kellen. *Effects of Hydrogen-Oxygen Torch Igniter Combustion Applied to an ABS/GOx Hybrid Rocket System*. 2022. University of California, Davis, Master’s Thesis.

[59] “Hydrogen Fuel Cell Engines and Related Technologies Course Manual.” *Office of Energy Efficiency & Renewable Energy*, 7 Mar. 2014,

https://www.energy.gov/eere/fuelcells/downloads/hydrogen-fuel-cell-engines-and-related-technologies-course-manual.

[60] “Hydrogen explained.” *U.S. Energy Information Administration*, 21 Jan. 2022, https://www.eia.gov/energyexplained/hydrogen/production-of-hydrogen.php#:~:text=The%20two%20most%20common%20methods,electrolysis%20.

[61] “Hydrogen Production: Natural Gas Reforming.” *Office of Energy Efficiency and Renewable Energy*, https://www.energy.gov/eere/fuelcells/hydrogen-production-natural-gas-reforming.

[62] Coward, H.F. and G.W. Jones. *Limits of Flammability of Gases and Vapors*. United States Department of the Interior, 1952.

[63] Cecere, D. et al. “A review on hydrogen industrial applications.” *International Journal of Hydrogen Energy*, vol. 39, no. 20, Elsevier Ltd, 3 July 2014, pp. 10731-10747.

[64] “Hydrogen Storage.” *Office of Energy Efficiency and Renewable Energy*, https://www.energy.gov/eere/fuelcells/hydrogen-storage.

[65] Oztan, Cagri and Victoria Coverstone. “Utilization of additive manufacturing in hybrid rocket technology: A review.” *Acta Astronautica*, vol. 180, Mar. 2021, pp. 130-140.

[66] Dinesh, Mengu and Rajiv Kumar. “Utility of Multiprotrusion as the Performance Enhancer in Hybrid Rocket Motor.” *Journal of Propulsion and Power*, vol. 35, no. 5, Sep. 2019.

[67] Zdybal, Dominik et al. “Investigation of FDM-printed open-framework-reinforced helical PEWAX grains as a robust, high regression hybrid rocket fuel.” *AIAA Scitech 2021 Forum*, 4 Jan. 2021.

[68] Deopura, B.L. and N.V. Padaki. “Synthetic Textile Fibres: Polyamide, Polyester and Aramid Fibres.” *Textiles and Fashion*, Elsevier Ltd, 2015.

[69] “Ertalon® 6 PLA.” *Mitsubishi Chemical Advanced Materials*, Mitsubishi Chemical Group, https://www.mcam.com/jp-en/products/engineering-plastics/engineering-80-160/extruded-cast-nylons/ertalonr-6-pla-pa6/.

[70] Whitmore, Stephen A., et al. “Comparing Hydroxyl Terminated Polybutadiene and Acrylonitrile Butadiene Styrene as Hybrid Rocket Fuels.” *Journal of Propulsion and Power*, vol. 29, no. 3, 2013, pp. 582–592.

[71] Banks, Joseph. “CEA Application Info.” *NASA Glenn Research Center*, 28 Oct. 2021, https://www1.grc.nasa.gov/research-and-engineering/ceaweb/topicshome/.

[72] Conversano, Ryan W. et al. “SmallSat Missions Enabled by Paired Low-Thrust Hybrid Rocket and Low-Power Long-Life Hall Thruster.” *California Institute of Technology Jet Propulsion Laboratory*, 2019.

[73] Jens, Elizabeth T. et al. “Low Pressure Ignition Testing of a Hybrid SmallSat Motor.” *California Institute of Technology Jet Propulsion Laboratory*.

[74] Simurda, Laura and Gregory Zilliac. “Continued Testing of a High Performance Hybrid Propulsion System for Small Satellites.” *AIAA Propulsion and Energy Forum*, July 2015.

[75] Nigar, Baris et al. “Understanding mechanical failure of graphite rocket nozzle throats under thermal stresses.” *Aerospace Science and Technology*, vol. 119, Dec. 2021.

Appendix A

K-Factors for Aalborg Mass Flow Meters

ACTUAL GAS	K FACTOR Relative to N_2	Cp [Cal/g]	Density [g/l]
Deuterium D_2	1.00	1.722	1.799
Diborane B_2H_6	.4357	.508	1.235
Dibromodifluoromethane CBr_2F_2	.1947	.15	9.362
Dichlorodifluoromethane (Freon-12) CCl_2F_2	.3538	.1432	5.395
Dichlofluoromethane (Freon-21) $CHCl_2F$	.4252	.140	4.592
Dichloromethylsilane $(CH_3)_2SiCl_2$	.2522	.1882	5.758
Dichlorosilane SiH_2Cl_2	.4044	.150	4.506
Dichlorotetrafluoroethane (Freon-114) $C_2Cl_2F_4$	.2235	.1604	7.626
1,1-Difluoroethylene (Freon-1132A) $C_2H_2F_2$	.4271	.224	2.857
Dimethylamine $(CH_3)_2NH$	.3714	.366	2.011
Dimethyl Ether $(CH_3)_2O$	.3896	.3414	2.055
2,2-Dimethylpropane C_3H_{12}	.2170	.3914	3.219
Ethane C_2H_6	.50	.420	1.342
Ethanol C_2H_6O	.3918	.3395	2.055
Ethyl Acetylene C_4H_6	.3225	.3513	2.413
Ethyl Chloride C_2H_5Cl	.3891	.244	2.879
Ethylene C_2H_4	.60	.365	1.251
Ethylene Oxide C_2H_4O	.5191	.268	1.965
Fluorine F_2	.9784	.1873	1.695
Fluoroform (Freon-23) CHF_3	.4967	.176	3.127
Freon-11 CCl_3F	.3287	.1357	6.129
Freon-12 CCl_2F_2	.3538	.1432	5.395
Freon-13 $CClF_3$	.3834	.153	4.660
Freon-13B1 $CBrF_3$	.3697	.1113	6.644
Freon-14 CF_4	.4210	.1654	3.926
Freon-21 $CHCl_2F$	.4252	.140	4.592
Freon-22 $CHClF_2$	.4589	.1544	3.858
Freon-113 CCl_2FCClF_2	.2031	.161	8.360
Freon-114 $C_2Cl_2F_4$	.2240	.160	7.626
Freon-115 C_2ClF_5	.2418	.164	6.892
Freon-C318 C_4F_8	.1760	.185	8.397
Germane GeH_4	.5696	.1404	3.418
Germanium Tetrachloride $GeCl_4$	.2668	.1071	9.565
Helium He	1.454	1.241	.1786
Helium He-1 (>50 L/min)	2.43	1.241	.1786
Helium He-2 (>10-50 L/min)	2.05	1.241	.1786
Hexafluoroethane C_2F_6 (Freon-116)	.2421	.1834	6.157
Hexane C_6H_{14}	.1792	.3968	3.845
Hydrogen H_2-1	1.0106	3.419	.0899
Hydrogen H_2-2 (>10-100 L)	1.35	3.419	.0899
Hydrogen H_2-3 (>100 L)	1.9	3.419	.0899

ACTUAL GAS	K FACTOR Relative to N_2	Cp [Cal/g]	Density [g/l]
Hydrogen Bromide HBr	1.000	.0861	3.610
Hydrogen Chloride HCl	1.000	.1912	1.627
Hydrogen Cyanide HCN	.764	.3171	1.206
Hydrogen Fluoride HF	.9998	.3479	.893
Hydrogen Iodide HI	.9987	.0545	5.707
Hydrogen Selenide H_2Se	.7893	.1025	3.613
Hydrogen Sulfide H_2S	.80	.2397	1.520
Iodine Pentafluoride IF_5	.2492	.1108	9.90
Isobutane $CH(CH_3)_3$	.27	.3872	3.593
Isobutylene C_4H_8	.2951	.3701	2.503
Krypton Kr	1.453	.0593	3.739
Methane CH_4	.7175	.5328	.715
Methane CH_4-1 (>10 L/min)	.75	.5328	.715
Methanol CH_3	.5843	.3274	1.429
Methyl Acetylene C_3H_4	.4313	.3547	1.787
Methyl Bromide CH_3Br	.5835	.1106	4.236
Methyl Chloride CH_3Cl	.6299	.1926	2.253
Methyl Fluoride CH_3F	.68	.3221	1.518
Methyl Mercaptan CH_3SH	.5180	.2459	2.146
Methyl Trichlorosilane $(CH_3)SiCl_3$	.2499	.164	6.669
Molybdenum Hexafluoride MoF_6	.2126	.1373	9.366
Monoethylamine $C_2H_5NH_2$	.3512	.387	2.011
Monomethylamine CH_3NH_2	.51	.4343	1.386
Neon NE	1.46	.246	.900
Nitric Oxide NO	.990	.2328	1.339
Nitrogen N_2	1.000	.2485	1.25
Nitrogen Dioxide NO_2	.737	.1933	2.052
Nitrogen Trifluoride NF_3	.4802	.1797	3.168
Nitrosyl Chloride NOCl	.6134	.1632	2.920
Nitrous Oxide N_2O	.7128	.2088	1.964
Octafluorocyclobutane (Freon-C318) C_4F_8	.176	.185	8.397
Oxygen O_2	.9926	.2193	1.427
Oxygen Difluoride OF_2	.6337	.1917	2.406
Ozone	.446	.195	2.144
Pentaborane B_5H_9	.2554	.38	2.816
Pentane C_5H_{12}	.2134	.398	3.219
Perchloryl Fluoride ClO_3F	.3950	.1514	4.571
Perfluoropropane C_3F_8	.174	.197	8.388
Phosgene $COCl_2$	.4438	.1394	4.418
Phosphine PH_3	.759	.2374	1.517

Appendix B

Nylon 6 Data and Safety Sheets

Polyamide

Ertalon® 6 PLA

MITSUBISHI CHEMICAL ADVANCED MATERIALS

PRODUCT DATA SHEET

Unmodified nylon 6 grade exhibiting characteristics which come very close to those of Ertalon® 66 SA. It combines high strength, stiffness and hardness with good creep and wear resistance, heat aging properties and machinability.

Physical properties (indicative values ■)

PROPERTIES			
Colour	-	-	White,Black,Blue,Yellow
Density	ISO 1183-1	g/cm³	1.15
Water absorption:			
- after 24 immersion in water of 23 °C (1)	ISO 62	%	0.65
- at saturation in water of 23 °C	-	%	6.5
Thermal Properties (2)			
Melting temperature (DSC, 10 °C/min)	ISO 11357-1/-3	°C	215
Glass transition temperature (DSC, 20 °C/min) - (3)	ISO 11357-1/-2	°C	
Thermal conductivity at 23 °C	-	W/(K.m)	0.29
Coefficient of linear thermal expansion:			
- average value between 23 and 60 °C	-	m/(m.K)	80 x 10-6
- average value between 23 and 100 °C	-	m/(m.K)	90 x 10-6
Temperature of deflection under load:			
- method A: 1.8 MPa	ISO 75-1/-2	°C	80
Max. allowable service temperature in air:			
- continuously : for min. 20,000 h (4)	-	°C	90
Min. service temperature (5)	-	°C	-30
Flammability (6):			
- according to UL 94 (3 mm thickness)	-	-	HB
Mechanical Properties at 23 °C (7)			
Tension test (8):			
- tensile strength (9)	ISO 527-1/-2	MPa	88
- tensile strain at yield(9)	ISO 527-1/-2	%	5
- tensile strain at break (9)	ISO 527-1/-2	%	25
- tensile modulus of elasticity (10)	ISO 527-1/-2	MPa	3600
Compression test (11):			
- compressive stress at 1 / 2 / 5 % nominal strain (10)	ISO 604	MPa	34 / 64 / 93
Flexural test (12):			
- flexural strength	ISO 178	MPa	121
- flexural modulus of elasticity	ISO 178	MPa	3280
Charpy impact strength - unnotched (13)	ISO 179-1/1eU	kJ/m²	no break
Charpy impact strength - notched	ISO 179-1/1eA	kJ/m²	3
Rockwell M-hardness (14)	ISO 2039-2	-	88
Dynamic Coefficient of Friction (-)	ISO 7148-2 (15)	-	0.4-0.6
Wear rate	ISO 7148-2 (15)	µm/km	12
Electrical Properties at 23 °C			
Electric strength (16)	IEC 60243-1	kV/mm	25
Volume resistivity	IEC 60093	Ohm.cm	>10E 14
Surface resistivity	ANSI/ESD STM 11.11	Ohm/sq.	>10E13
Relative permittivity ε_r : - at 1 MHz	IEC 60250	-	3.20
Dielectric dissipation factor tan δ: - at 1 MHz	IEC 60250	-	0.016

Note: 1 g/cm³ = 1,000 kg/m³ ; 1 MPa = 1 N/mm² ; 1 kV/mm = 1 MV/m.

Legend:
1) According to method 1 of ISO 62 and done on discs Ø 50 mm x 3 mm.
2) The figures given for these properties are for the most part derived from raw material supplier data and other publications.
3) Values for this property are only given here for amorphous materials and for materials that do not show a melting temperature (PBI, PAI, PI).
4) Temperature resistance over a period of min. 20,000 hours. After this period of time, there is a decrease in tensile strength – measured at 23 °C – of about 50 % as compared with the original value. The temperature value given here is thus based on the thermal-oxidative degradation which takes place and causes a reduction in properties. Note, however, that the maximum allowable service temperature depends in many cases essentially on the duration and the magnitude of the mechanical stresses to which the material is subjected.
5) Impact strength decreasing with decreasing temperature, the minimum allowable service temperature is practically mainly determined by the extent to which the material is subjected to impact. The value given here is based on unfavourable impact conditions and may consequently not be considered as being the absolute practical limit.
6) These estimated ratings, derived from raw material supplier data and other publications, are not intended to reflect hazards presented by the material under actual fire conditions. There is no 'UL File Number' available for these stock shapes.
7) Most of the figures given for these mechanical properties of the materials are average values of tests run on dry test specimens machined either out of plate 15-20 mm thick or rod diameter 40-50mm, the test specimens were then taken from the stock shape with their length in longitudinal direction (parallel to the extrusion direction).
8) Test specimens: Type 1 B
9) Test speed: either 5 or 50 mm/min [chosen acc. to ISO 10350-1 as a function of the ductile behaviour of the material (tough or brittle)
10) Test speed: 1 mm/min.
11) Test specimens: cylinders Ø 8 mm x 16 mm
12) Test specimens: bars 4 mm (thickness) x 10 mm x 80 mm ; test speed: 2 mm/min ; span: 64 mm.
13) Pendulum used: 4 J.
14) Measured on 10 mm thick test specimens.
15) Test procedure similar to Test Method A: "Pin-on-disk" as described in ISO 7148-2, Load 3MPa, sliding velocity= 0,33 m/s, mating plate steel Ra= 0.7-0.9 µm, tested at 23°C, 50%RH.
16) Electrode configuration: ⌀ 25 mm / ⌀ 75 mm coaxial cylinders ; in transformer oil according to IEC 60296 ; 1 mm thick test specimens.

This table is a valuable help in the choice of a material. The data listed here fall within the normal range of product properties of dry material. However, they are not guaranteed and they should not be used to establish material specification limits nor used alone as the basis of design.

It has to be noted that reinforced and filled material shows an anisotropic behaviour (properties differ when measured parallel and perpendicular to the manufacturing direction).

Ertalon® is a registered trademark of Mitsubishi Chemical Advanced Materials.

Ertalon® 6 PLA PA6

MITSUBISHI CHEMICAL ADVANCED MATERIALS

PRODUCT HANDLING INFORMATION SHEET

1. Supplier

Mitsubishi Chemical Advanced Materials
I.P. Noord – Galgenveldstraat 12
B – 8700 Tielt
Tel.: +32/(0)51/42 35 11
Fax: +32/(0)51/42 33 00

2. Product description

Commercial product name Ertalon® 6 PLA PA6
These products are '**articles**' according to the Regulation (EC) No 1907/2006 (REACH).

Material characterization cast polyamide 6 [PA 6]

3. Product characteristics

		Test methods
Form:	semi-finished products (round rods, sheets, plates, profiles) / finished parts machined from semi-finished products	
Colour:	natural (ivory) / black / blue	
Odour:	odourless	
Density:	1.15 g/cm³	ISO 1183-1
Melting temperature:	215 °C	ISO 11357-1/-3
Glass transition temperature:	-	ISO 11357-1/-2
	Values for this property are only given here for amorphous materials and not for semi-crystalline ones	
Thermal decomposition:	> 350 °C	
Self-ignition temperature:	> 400 °C	ASTM D 1929
Solubility in water:	insoluble	

4. Handling and storage

Machining: During machining of the semi-finished products, evacuate swarf to prevent slipping or tripping hazard and observe the maximum allowable concentration of dust levels on the workplace which apply in your country. Wear safety goggles during machining.

Storage: The products shall be stored indoors in a normal environment (air at 10 - 30°C / 30 - 70% RH) and kept away from any source of degradation such as sunlight, UV-lamps, chemicals (direct or indirect contact), ionising radiation, flames, etc. Dimensional changes (camber, warpage, shrinkage …) of the products as well as slight colour shifts of the external surfaces can occur with time. The latter does generally not pose a problem in case of semi-finished products since the surface-layer is mostly removed anyway upon machining them into finished parts.
The properties of materials which are prone to water absorption, e.g. polyamides, may change significantly with storage time as a result of water absorbed from the environment (this effect depends very much on shape and size of the products, the relative humidity and temperature of the environment and the time). However, this water absorption phenomenon being a reversible one, the original material properties can if necessary be restored by drying them.

Safety measures: Standard industrial safety recommendations shall be observed.
Temperatures above the melting temperature shall be avoided.

Please also note the disclaimer on page 2 of this document.

5. Fire-fighting measures

Suitable extinguishing media: Water, foam, dry chemical, CO_2. Adapted to the nature and extend of fire.

Hazardous decomposition products:
The main products formed in case of overheating and combustion carbon monoxide, carbon dioxide, nitrogen oxide (NOx) and traces of hydrogen cyanide and ammonia. Formation of further hazardous decomposition products depends upon the fire conditions and cannot be excluded.

Special protective equipment: Firemen should wear self-contained breathing apparatus and protective clothing to prevent contact with skin and/or eyes. If exposed to combustion fumes in a high concentration, bring the victim into fresh air. If molten material contacts skin, cool rapidly with cold water and obtain medical attention for removal of adhering material and treatment of the burn.

6. Disposal considerations

According to the **'European Waste Catalogue and Hazardous Waste List'**, uncontaminated waste from the products is not classified as hazardous. The following six-digit codes can be used:

07 02 13	waste plastic from the manufacture, formulation, supply and use of plastics
12 01 05	plastic shavings and turnings
16 01 19	plastic, from end-of-life vehicles from different means of transport (including off-road machinery) and wastes from dismantling of end-of-life vehicles and vehicle maintenance
17 02 03	plastic construction and demolition wastes
20 01 39	plastics from municipal wastes (household waste and similar commercial, industrial and institutional wastes)

Waste disposal: When recycling is not feasible, waste disposal by incineration or landfill can be applied. Disposal methods shall conform to local or other government regulations.
The products do not contain cadmium pigments or cadmium stabilisers. They are not biologically degradable, but based on the present state of knowledge no negative effects on the environment may be anticipated.

7. Marking and transport information

Classification and labelling: Hazard warning labelling in accordance with relevant EC-Directives is not required.

International transport regulations:
Not applicable

8. Other information

Consult the Mitsubishi website for the latest information on the Mitsubishi Chemical Advanced Material products (product data sheets, delivery programme, machining instructions, chemical resistance, regulatory information …) as well as for our statements concerning the European Regulation (EC) No 1907/2006 (REACH).